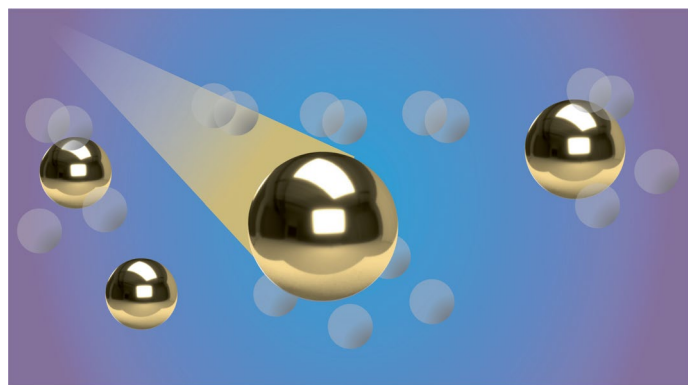


Strategies to improve hydrogen activation on gold catalysts

Nikolaos Dimitratos^{1,2}, Gianvito Vilé³, Stefania Albonetti^{1,2}, Fabrizio Cavani^{1,2}, Jhonatan Fiorio⁴, Núria López⁵, Liane M. Rossi⁶ & Robert Wojcieszak^{7,8}✉

Abstract

Catalytic reactions involving molecular hydrogen are at the heart of many transformations in the chemical industry. Classically, hydrogenations are carried out on Pd, Pt, Ru or Ni catalysts. However, the use of supported Au catalysts has garnered attention in recent years owing to their exceptional selectivity in hydrogenation reactions. This is despite the limited understanding of the physicochemical aspects of hydrogen activation and reaction on Au surfaces. A rational design of new improved catalysts relies on making better use of the hydrogenating properties of Au. This Review analyses the strategies utilized to improve hydrogen–Au interactions, from addressing the importance of the Au particle size to exploring alternative mechanisms for H₂ dissociation on Au cations and Au–ligand interfaces. These insights hold the potential to drive future applications of Au catalysis.



Sections

Introduction

Hydrogenations on Au

Improving Au–hydrogen interactions

Conclusion and outlook

¹Dipartimento di Chimica Industriale “Toso Montanari”, Alma Mater Studiorum Università di Bologna, Bologna, Italy. ²Center for Chemical Catalysis-C3, Alma Mater Studiorum Università di Bologna, Bologna, Italy.

³Department of Chemistry, Materials and Chemical Engineering “Giulio Natta”, Politecnico di Milano, Milano, Italy. ⁴Technische Universität Dresden, School of Science, Faculty of Chemistry and Food Chemistry, Dresden, Germany.

⁵Institute of Chemical Research of Catalonia, The Barcelona Institute of Science and Technology, Tarragona, Spain. ⁶Departamento de Química Fundamental, Instituto de Química, Universidade de São Paulo, São Paulo, Brazil. ⁷Univ. Lille, CNRS, Centrale Lille, Univ. Artois, UMR 8181 - UCCS - Unité de catalyse et chimie du solide, Lille, France. ⁸Present address: Université de Lorraine and CNRS, L2CM UMR 7053, Nancy, France.

✉e-mail: robert.wojcieszak@univ-lille.fr

Introduction

Catalytic transformations involving molecular hydrogen (H_2) are named hydrogenations, and they are common in the chemical industry. For a long time, it was believed that only certain metals, such as platinum (Pt), palladium (Pd) and nickel (Ni), possessed the catalytic ability to dissociate H_2 efficiently. These metals have been extensively used in industrial processes owing to their ability to facilitate hydrogenation reactions. However, issues related to overhydrogenation with Ni catalysts and the high cost and limited availability of Pt and Pd have prompted researchers to explore alternative catalysts. In this pursuit, scientists discovered that gold (Au), typically considered inert, can catalyse the activation of H_2 and other H-donors, and exhibit remarkable catalytic properties in hydrogenation reactions^{1,2}. This finding has shattered a long-standing limitation in the field and opened up new possibilities for increasing the selectivity of various hydrogenation processes (Box 1).

Heterogenous catalysts are used in many industrial processes^{3–5}, and they often involve finely dispersed metallic nanoparticles (NPs). One such catalytic system consists of Au NPs dispersed on solid carriers⁶, whose usefulness was initially demonstrated in selective carbon monoxide (CO) oxidation reactions^{7–9}. Dispersing the Au NPs in this way provides a large number of low-coordination surface sites that offer improved catalytic properties compared with conventional Au surfaces^{8,10}. The enhanced activity and selectivity are linked to the quantum effects unique to the nanoscale. When Au NPs are very small (<2 nm in diameter), a notable quantization occurs to the conduction band. In these quantum-sized NPs, many of the physical and chemical properties of Au are fundamentally altered¹¹. For example, quantum-sized Au NPs show multiple optical absorption peaks in the optical spectrum, whereas a single surface plasmon resonance peak at 520 nm is observed for larger spherical Au NPs. In addition, removing or adding one Au atom can alter the electronic properties of Au NPs owing to the strong quantum confinement effect¹¹. Together with Au–support interactions, these quantum effects are responsible for the unusual catalytic properties of Au, which allow Au NPs to activate small molecules such as CO at low temperatures. The discovery that very small Au particles, specifically those with sizes smaller than 10 nm, can be a viable catalysts for hydrogenation reactions was a breakthrough in heterogeneous chemistry^{12–14}. Understanding the mechanisms by which hydrogen can be activated on Au is crucial to designing stable and efficient supported Au catalysts for hydrogenation reactions^{15,16}.

Generally, hydrogenation reactions on metal surfaces, including Au, proceed via the Horiuti–Polanyi mechanism, which involves the homolytic splitting of a hydrogen molecule adsorbed on the metal surface and the sequential transfer of each H atom to the reactive molecule. This critical activation step has been explored conducting Infrared, X-ray absorption fine structure and hydrogen–deuterium exchange experiments on supported Au NPs^{2,17–19}. By combining theory and experiment, the nature and structure of the active sites responsible for the adsorption and dissociation of molecular hydrogen are now well understood. The presence of the low-coordinated atoms located at the corner and edge of the Au particle is necessary for H_2 splitting on Au NPs^{2,17–20}. Hydrogen adsorption is only possible on low-coordinated atoms, whereas AuNPs become repulsive at high coordination numbers (>8). Despite these research efforts, some key questions remain concerning the charge transfer between the Au surface and the adsorbed H species, the presence of alternative hydrogen dissociation paths, and the degree of mobility of H species on the Au NPs²¹. The main challenge in using Au for hydrogenation reactions is its low efficiency in dissociating H_2 under standard conditions.

The important factors that make bulk Au the most noble metal and an ineffective species for hydrogen dissociation have to do with the largest orbital overlap with the adsorbed hydrogen and highly filled antibonding adsorbate–metal *d* states²².

In this Review, we will discuss the main strategies to assess the hydrogenation activity of Au NPs and single atoms. We will focus our discussion on strategies that can enhance Au–H interactions and thus improve the hydrogenation ability of Au. This Review reports on hydrogenation and hydroconversion reactions using Au NPs and single atoms. Specifically, we highlight the most substantial advances concerning hydrogenation on Au-based catalysts of the past 5 years. Subsequently, we identify challenges to the design of more efficient Au formulations for the selective hydrogenation processes in heterogeneous and single-atom catalysis. Next, we discuss the chemical aspects of the catalytic reaction during the selective hydrogenation process and, finally, the theoretical aspects of hydrogenation on Au surfaces, including hydrogen dissociation and transfer. We hope to contribute to advancing the understanding of the relationships between reactions involving H_2 and Au catalysts in the catalysis and materials chemistry communities.

Hydrogenations on Au

The fundamental development of Au-based catalytic formulations^{16,23–25} and the enhancement of existing systems^{26–28} require a deep understanding of the impacts of active metals, supports, solvents, metal additives, co-catalysts and catalyst preparation methods, as well as the study of active sites. The catalytic performance of Au is substantially improved through the design of multi-phase formulations (bimetallic and promoted Au catalysts) as well as synthesis methodologies to enhance the active phase dispersion and modulate the size and localization of Au NPs within a support material. Theoretical investigations have provided insights into the mechanism of H_2 activation, hydride formation²⁹ and the adsorption of the substrates on both Au and oxide (playing the role of the support) surfaces. Furthermore, these studies have contributed to the understanding of reaction mechanisms in these systems, from homolytic to heterolytic H_2 dissociation (Box 2).

The development of Au catalysts remains hampered by a number of obstacles. For example, the ability to control and tune the chemical composition of Au and Au bimetallic NPs and/or nanoclusters is limited, especially when catalysts are prepared with traditional methods such as co-precipitation or co-impregnation of metal salts. These procedures frequently allow for limited control over the size and uniformity of the particles, leading to the formation of mixed particles that consist of both monometallic and bimetallic NPs. Another problem is the deactivation of the catalyst as a result of structure degradation, leaching and carbon deposition³⁰. The mechanisms underlying the degradation of the catalyst performances are still not fully understood and more attention is needed to mitigate the deactivation. Finally, various fundamental aspects of the mechanism remain incompletely understood, such as kinetic modelling, adsorption geometry and active-phase modelling.

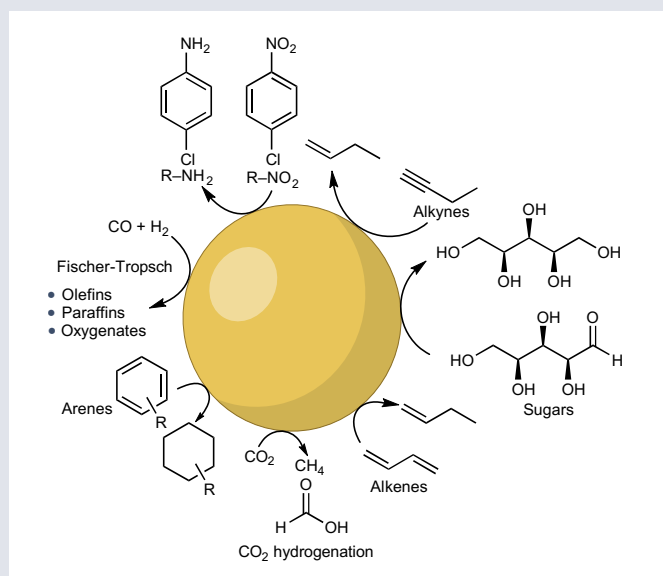
One motivation behind conducting research into catalysis on Au is the potential to enhance the efficiency of hydrogenation reactions. The design of nanostructured supported Au catalysts allows the development of catalyst systems characterized by high activity and selectivity, and excellent resistance to both chemical and structural degradation. One of the crucial parameters of catalyst design is the optimization of the structure of the active sites to enhance catalyst selectivity in hydrogenation reactions^{13,14}. In addition, although the mechanism of hydrogen adsorption on a pure Au surface is well established, the fate

Box 1

The importance of hydrogenation reactions in the chemical industry

Hydrogenation reactions are fundamental processes in the chemical industry with widespread applications. Catalytic hydrogenation was first performed in 1897 by Sabatier, who described the reduction of ethylene using metals such as Ni, Co and Fe (1912 Nobel Prize in Chemistry)¹⁰⁷. The first large-scale hydrogenation process was the hydrogenation of fatty acids and their glycerides using a Ni catalyst in 1909 by Crasfield & Sons LTD, England¹⁰⁸. The addition of hydrogen gas (H_2) to a compound in the presence of a catalyst can lead to significant change in the molecular structure of the substrate. One of the most prevalent hydrogenation reactions involves reducing unsaturated compounds. When hydrogen gas reacts with a molecule containing double bonds, these bonds become saturated, leading to the formation of single bonds. This procedure is extensively utilized in the production of saturated hydrocarbons, including the conversion of unsaturated vegetable oils into solid fats, such as margarine. In addition to reducing double-bonds and triple-bonds, hydrogenation reactions are utilized in a number of other functional group conversions. For instance, the hydrogenation of carbonyl compounds, such as aldehydes and ketones, leads to the formation of alcohols. This transformation is essential in the production of pharmaceuticals, flavourings and fragrances. Heterogeneous catalytic hydrogenation can be performed using metals such as Ni, Ru, Rh and Pd. In addition, numerous catalytic hydrogenation processes

can also be performed on Au-based catalysts, some of which are presented below.



of hydrogen species after dissociation from the metal is not completely understood, including the degree of H atom mobility on Au particles²¹. Several uncertainties remain around the reactivity of specific Au atoms and the origin of the dissociation (activated and/or spontaneous). Theoretical investigations have helped develop more efficient Au-based catalysts for hydrogenations, such as open surfaces as Au(100) and low-coordinated sites (edges or defects) that enhance Au activity³¹.

A fundamental understanding of the interactions of hydrogen with Au as well as those between the Au and ligand and between Au and support are necessary to rationalize the performance of the catalysts, from the nanolevel to the single-atom catalyst (SAC) level^{32–34}. For example, in the semihydrogenation of alkynes, Au was predicted to exhibit a higher selectivity towards alkenes than Pd by density functional theory (DFT) calculations, and this prediction was also confirmed experimentally³¹. In hydrogenations on Pd catalysts, both triple and double C–C bonds are adsorbed at the same rate; therefore, a competition between these two types of bonds arises, resulting in a mix of products³¹. Conversely, the triple C–C bonds of alkynes are preferentially adsorbed and are subsequently activated on Au³¹. In other words, triple C–C bonds can be preferentially hydrogenated and the alkene products can desorb from the Au surface, avoiding further hydrogenation³¹. This high chemoselectivity of supported small Au NPs enabled the hydrogenation of α,β -unsaturated aldehydes to the corresponding unsaturated alcohols^{35,36} and the deprotection of epoxides via deoxygenation to the corresponding alkenes³⁷, in both cases preserving the C=C bonds.

Improving Au–hydrogen interactions

The activation of hydrogen on Au (leading to hydrogen dissociation) is considered the rate-determining step in Au-catalysed hydrogenations²². In this context, several strategies have been developed to enhance the rate of H_2 dissociation to improve the catalytic efficiency of supported Au catalysts (Fig. 1). The main approaches are the heterolytic hydrogen dissociation occurring on Au interacting with nitrogen-containing ligands³⁸ (Fig. 1b) or at the metal–support interface, in the case of strong metal–support interactions³⁹ (SMSIs; Fig. 1c). H_2 dissociation could be also induced by hot electrons generated by plasmon enhancement⁴⁰ (Fig. 1d) or at single Au atoms⁴¹ (Fig. 1e), as well as by alloying Au with a second metal as schematically represented in Fig. 1f. Here, we discuss the most important approaches to enhancing the reactivity of Au in hydrogenation reactions.

Ligands

Auxiliary ligands can help enhance selectivity in heterogeneous catalysis. In the hydrogenation reaction on Au NPs, the addition of certain ligands has been demonstrated to lead to enhanced activity in the selective hydrogenation of alkynes to *cis*-alkenes (Fig. 2a). An inactive silica-supported Au NP catalyst (Au/SiO₂) exhibited a substantial increase in activity in the presence of various nitrogen-containing ligands³⁸. In the presence of piperazine, for example, the Au catalyst gained activity and selectivity towards the alkene, even when the reaction was allowed to continue to the full conversion (Fig. 2b),

Box 2

The complexity of the H–M interactions

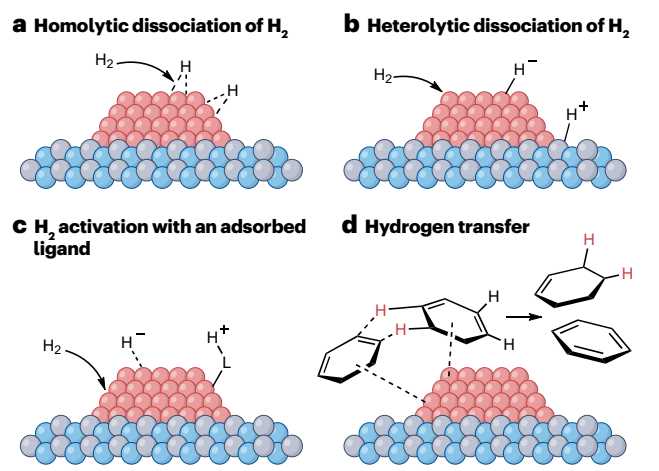
Different hydrogen activation pathways can occur on clean-surface Au nanoparticles^{109,110}, as indicated in the figure. The homolytic dissociation of H₂ to produce atoms on low-coordinated Au atoms is well documented from the theoretical point of view (part **a**). Depending on the electronegativity of metals, these bonds can be more or less polarized. Highly electronegative metals (such as Au) form mostly covalent bonds with hydrogen (M–H). It is worth noting that chemisorption of hydrogen is almost always exothermic (except on Au and Ag surfaces).

Heterolytic dissociation of hydrogen is more commonly observed in situations in which a metal hydride is formed after proton transfer to the support or substrate (part **b**). Typically, metal hydrogenation catalysts dissociate H₂ with a proton transfer to a strong conjugate base. This process involves the formation of proton–hydride pairs.

A third possibility is the activation of hydrogen molecules with a ligand adsorbed on the Au surface (part **c**) and the subsequent formation of a new active species (H–L, where L=ligand)¹⁰⁹.

Unlike the classical mechanisms of hydrogenation that involve the binding of substrates on the metal surface, a final mechanism, hydrogen transfer, enables the hydrogenation of sterically hindered substrates (part **d**). This ‘outer sphere’ hydrogenation mechanism involves several steps (adsorption of reactant, adsorption of H₂, complex formation, hydrogen transfer and desorption) with the overall

transfer of a proton to an unsaturated substrate. This mechanism can be used to convert complex molecules, and it is thus useful for the generation of pharmaceutically relevant structures. It also does not require gaseous hydrogen, but it can utilize another liquid hydrogen donor such as ethanol, isopropanol or formic acid^{109,110}.



Parts **a–d** adapted with permission from ref. 109, ACS.

a situation in which most catalysts lose selectivity. Ligands with two nitrogen donors exhibited an increased ability to lower the energy barrier (activation energy) of the heterolytic dissociation of H₂ and afforded an increase in the Au hydrogenation reaction rate (Fig. 2d). Ligands with only one nitrogen donor (red squares in Fig. 2d), such as pyrazine, are capable of splitting H₂, but they do not display the same catalytic performance as those with two nitrogen donors, because they easily leave the Au surface after protonation and do not complete the H-transfer steps required to complete the catalyst cycle. According to DFT studies, the ligand–Au interface is responsible for the H₂ dissociation through a heterolytic mechanism. Initially, the H₂ molecule approaches the ligand–Au interface. The H₂ molecule is then cleaved heterolytically, the proton is transferred to the amine ligand, forming a quaternary N centre, and the hydride goes to the Au surface. Subsequently, the H species adsorbed on Au can be transferred to the adsorbed alkyne. The catalytic cycle is completed once the proton is transferred from the ligand to the organic moiety, which regenerates the amine ligand; a process followed by the desorption of the alkene. A number of experimental parameters needed to be optimized to achieve an effective hydrogenation reaction. These included identifying a ligand with optimal basicity for the lowest input energy for hydrogen activation, which also did not bind too strongly, thus avoiding the catalyst site’s getting blocked, and did not cause metal leaching that affected the stability of the Au surface³⁸. Piperazine was selected as the best ligand, among 19 amines tested, to promote the catalytic hydrogenation of alkynes on Au NP catalyst³⁸.

The Au–ligand catalytic system can be considered a frustrated Lewis pair analogue⁴². Other studies in the literature reported similar observations when Au NPs were combined with nitrogen-containing^{43,44} or phosphorous-containing⁴⁵ ligands for hydrogenations.

It is noteworthy that the presence of nitrogen atoms in graphitic carbon materials (N-doped carbon) prepared through 1,10-phenanthroline pyrolysis has shown a similar effect to that described above on the properties of Au NP catalysts, specifically in catalytic hydrogenation reactions. The basic N atoms of the carbon support play an important role in hydrogen activation (in heterolytic mode) at the Au–N-doped carbon interface. In this context, Au NPs coated with N-doped carbon materials supported on titania (Au@N-doped C/TiO₂) showed enhanced catalytic activity (Fig. 2c) when compared with uncoated titania-supported Au NPs catalyst (Au/TiO₂) for alkyne semihydrogenation⁴³. The main advantage compared with the previous study is that the catalyst is fully heterogeneous, meaning it can be reused, and the products can be easily separated by filtration. The nitrogen atoms present in the carbon material are part of the catalyst’s composition and do not need to be added as external ligands, as it was the case in the previous study³. A combination of experimental and computational studies revealed an N-assisted heterolytic H₂ activation mechanism (Fig. 2e). The creation of an interface that mimicked the N-doped (pyridinic) graphene-like sheets experimentally observed after pyrolysis produced a system that exhibited a behaviour similar to that of a frustrated Lewis pair that enables an essentially barrierless heterolytic dissociation of H₂ (transition state C (TS-C) in Fig. 2e). The frustrated Lewis pair is formed due

to the absence of a direct interaction between Au and the lone pair of the nitrogen, allowing a unique interface that promotes the heterolytic cleavage of H_2 ⁴³. Subsequently, the catalytic cycle is completed by two H-transfer steps (transition states D and E (TS-D and TS-E) in Fig. 2e) and product desorption, closing the catalytic cycle and regenerating the initial species A. The mechanism illustrates the major role of N-heteroatoms in H_2 activation.

In another example, verified by DFT calculations, Lewis bases, such as NH_3 , adsorbed on four different models for Au surfaces and clusters (Au(111)-close-packed, Au(211)-step-edged, Au(111)-single atom and Au_{38} cluster) were able to generate hydrides (H^-) and protons (H^+) through heterolytic H_2 dissociation. The generated hydride and proton can then be concertedly transferred to CO_2 to produce formic acid in all four Au models⁴⁶. The cooperation between Au and adsorbed basic ligands has also been utilized in the hydrogenation of other organic molecules, including quinolines⁴⁷, imines or nitriles⁴⁴, and aldehydes^{48,49}.

Au–support interactions

Another strategy to enhance the hydrogenation activity of Au is to utilize SMSIs, which is a term that refers to the interactions that occur between metal NPs or atoms and the support material in heterogeneous catalysts^{27,28}. These interactions play a critical role in the performance and stability of the catalysts and are particularly important for catalysts supported on oxides, such as SiO_2 , Al_2O_3 or TiO_2 . In catalysis, SMSIs can lead to several effects, such as the promotion of the dispersion of metal NPs on the support and the prevention of their aggregation, thus leading to an increase in the surface area and in the number of active sites. They enhance the stability of the metal NPs on the support, preventing their sintering or leaching during the catalytic process²⁸. In addition, SMSIs can influence the adsorption and activation of reactant molecules, affecting the selectivity of the catalytic reaction. Thus, by taking advantage of SMSIs, the support stabilizes heterolytically dissociated hydrogen. This outcome arises from the intimate proximity between the support

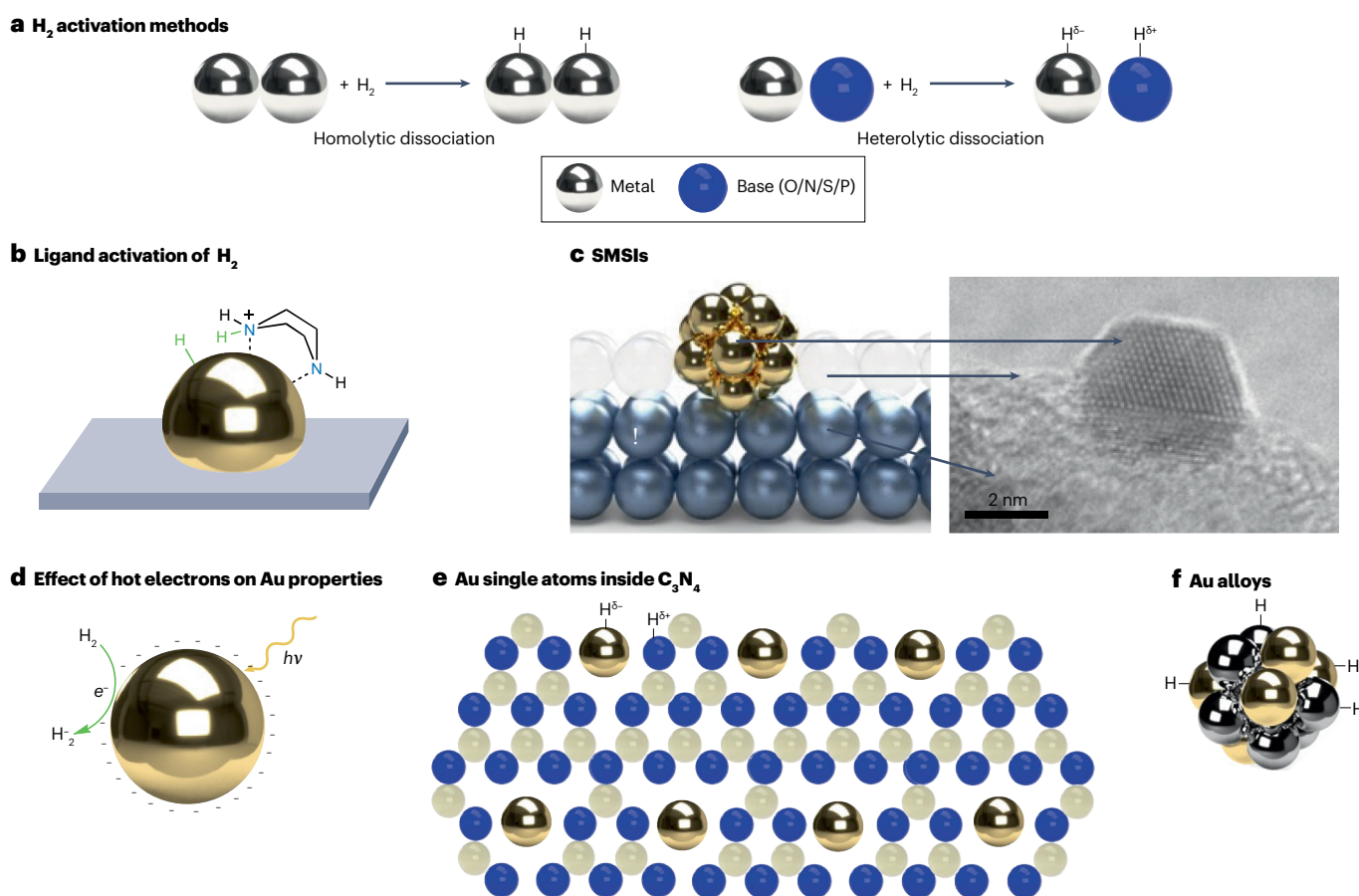
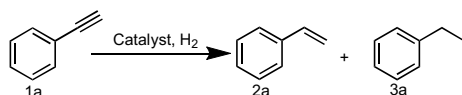


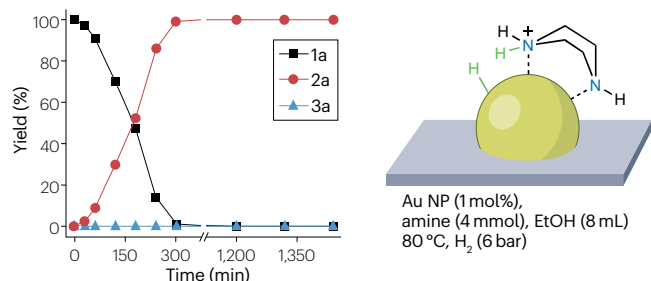
Fig. 1 | Types of H_2 activation on heterogeneous Au catalysts and strategies to enhance H_2 dissociation on Au. **a**, The two types of H_2 activation that may occur on Au. **b**, Ligands containing N or P adsorbed on the Au surface can heterolytically dissociate hydrogen due to the interactions between ligand and hydrogen. **c**, Strong metal–support interactions (SMSIs) can modify the electronic properties of Au and provide the necessary energy for hydrogen dissociation. In the figure is reported one example of strong SMSIs observed in the case of Au supported on $\text{TiO}_2@/\text{SiO}_2$. The partial encapsulation of Au by TiO_2 (white spheres) can be observed. Blue spheres represent SiO_2 . On the right

is a transmission electron microscopy (TEM) image of the catalyst represented on the left. **d**, Schematic representation of hydrogen adsorption and charge distribution on Au induced by hot electrons. **e**, Schematic representation of an Au single atom inside of the C_3N_4 structure (blue circles represent nitrogen atoms and grey circles represent carbon atoms). **f**, Alloying Au (gold-coloured spheres) with another metal such as Pt or Pd (metallic grey spheres) allows obtaining highly efficient hydrogenation catalysts. H_2 can easily dissociate on Pd or Pt, and it can then migrate to Au thanks to the spillover phenomenon. The gold-coloured spheres represent Au particles (parts **b–d**) or Au single atoms (parts **e** and **f**).

a Catalytic hydrogenation of phenylacetylene to styrene and ethylbenzene



b Reaction course with Au/SiO₂ catalyst and piperazine



c Reaction course with Au@N-doped carbon/TiO₂ catalyst

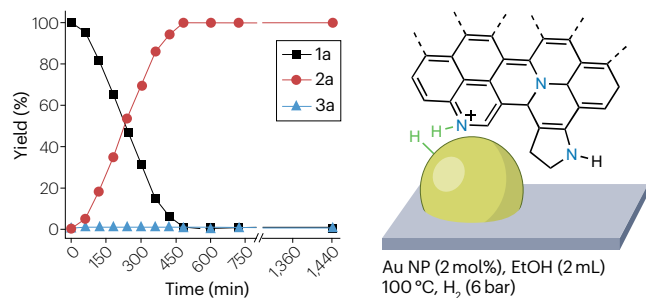
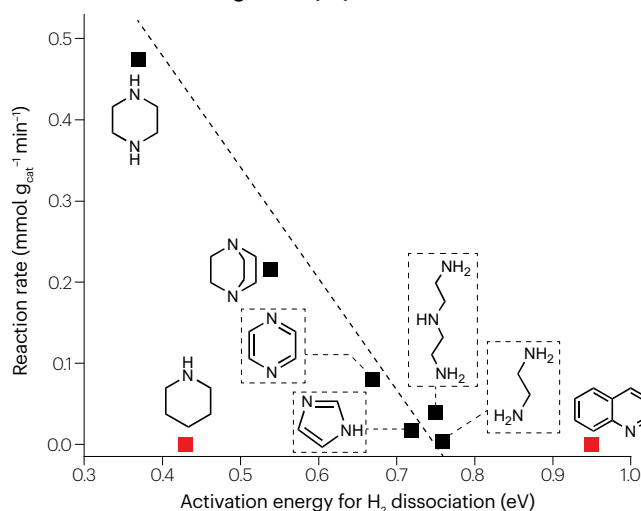
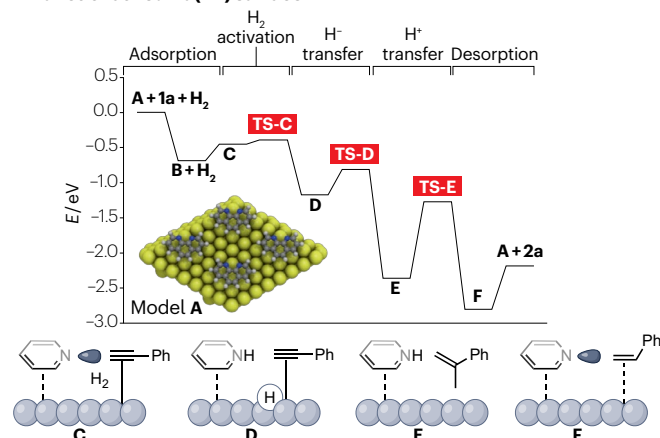


Fig. 2 | Selective hydrogenation on Au catalysts in the presence of ligands and in the case of Au-N-doped catalyst. a, Reaction scheme of the catalytic hydrogenation of phenylacetylene (1a) to styrene (2a) and ethylbenzene (3a). **b**, Time course of the hydrogenation of 1a catalysed by Au nanoparticles (NPs) supported on silica (Au/SiO₂), in the presence of piperazine (amine). **c**, Time course of the hydrogenation of 1a catalysed by Au NPs coated with N-doped carbon materials supported on titania (Au@N-doped carbon/TiO₂). **d**, Experimental reaction rates versus computed activation energies for H₂ dissociation in a heterolytic mode at the N ligand–Au(III) interface. Black squares

d Experimental reaction rates vs computed activation energies for H₂ dissociation at the N ligand–Au(III) interface



e Computed reaction energy profile for hydrogenation on phenanthroline-functionalized Au(III) surface



refer to amines with two N-heteroatoms and red squares to amines with one N-heteroatom in their structures. **e**, Computed reaction energy profile for the hydrogenation of an alkyne on a phenanthroline-functionalized Au(III) surface. The inset represents an Au(III) surface functionalized with phenanthroline in a configuration parallel (flat) to the surface (surface model A). Colour coding: Au, yellow; N, blue; C, grey; H, white. EtOH, ethanol; TS, transition state. Reprinted with permission from ref. 38,43. Parts **b–c** adapted with permission from ref. 38, ACS. Part **d** adapted with permission from ref. 43, ACS. Part **e** reprinted with permission from ref. 43, ACS.

and the metal catalyst (Fig. 1c), fostering charge redistribution and electronic polarization. In hydrogenations, these factors collectively contribute to the enhanced stability of the dissociated hydrogen species. Heterolytic dissociation is much more energy-intensive than homolytic dissociation, as determined experimentally (17.36 eV versus 4.52 eV, respectively)^{50,51}. Therefore, the extra energy needs must be compensated via the creation of new bonds, setting a minimum level of charge separation for the process to occur efficiently⁵⁰. The interface of the oxide support can help enhance this heterolytic process^{39,52}. An illustration of this concept is represented by the case of TiO₂(110),

in which the presence of low-coordinated O₂ atoms adjacent to the Au clusters has been observed. This arrangement has the potential to facilitate the dissociation of molecular H₂, leading to the protonation of the oxygen atoms situated on the support⁵².

By contrast, the Au SACs supported on electron-rich cavities of N-doped carbon (such as graphitic carbon nitride obtained by the pyrolysis of organic amines—C₃N₄) dissociate H₂ homolytically⁴¹. The catalyst was suggested by DFT to be composed of Au^{δ+} (1 < δ < 3) species stabilized by oxidized pyridinic N atoms at the cavities from the N-doped carbon. The developed catalyst led to thermodynamically

more favoured H₂ activation than the stepped surface Au(211) (−1.13 eV versus −0.17 eV, respectively).

The structure-sensitivity (the kinetics is dependent on the particle size due to changes in the coordination of surface atoms with particle size) of Au can also promote catalysts. Small Au NPs supported on TiO₂ of around 3 nm exhibited a higher selectivity towards 3-vinylaniline (78%; side product being 3-ethylnitrobenzene, with 16%) than those of 9 nm (39% of 3-vinylaniline and 51% of 3-ethylnitrobenzene) in the hydrogenation of 3-nitrostyrene. In addition, a model catalyst containing Au particles of both sizes (3 nm and 9 nm) showed a moderate selectivity towards 3-vinylaniline (55%) at relatively high conversion (25%)⁵³. Nevertheless, the application of a reduction process to the Au catalysts resulted in enhanced selectivity for both particle sizes. In both cases, with particle sizes of 3 nm and 9 nm, the selectivity surpassed 95% after the reduction process. The main difference was that the catalyst with the larger Au NPs (9 nm) exhibited a substantially lower conversion (14.9%) than the catalyst with 3 nm Au NPs (or the combination of Au NPs of 3 and 9 nm, 15.4% and 24.8%, respectively), which maintained a high conversion level⁵³. By characterizing the catalysts by high-resolution transmission electron microscopy, it was found that the catalyst with the larger Au NPs (9 nm) had a larger degree of encapsulation, which reduced catalytic activity. In the case of the smaller Au NPs, only partial encapsulation was observed. This was explained by the surface tensions of the metal and support during the encapsulation process⁵³. Typically, the metal has a higher surface tension than the TiO₂ support, which is often observed experimentally. In the case of Au, its relatively low surface tension ($\gamma_{\text{Au}} = 1.51 \text{ J m}^{-2}$) has been considered as a hindrance for the formation of SMSIs⁵³. Recent discoveries of SMSIs in TiO₂-supported Au catalysts have challenged the value of the previously reported surface tension of TiO₂ (1.3–1.9 J m^{−2}) and raised questions about its potential overestimation⁵⁴. This opens up the possibility that Au may possess a higher surface tension than TiO₂, allowing it to be wetted by TiO₂ and leading to the encapsulation of Au NPs as a result of the minimization of their surface free energy. Furthermore, at the nanoscale, the size-dependence of surface tension plays an important role. Although both positive and negative correlations between surface tension and particle size have been observed, a positive correlation is more likely at high temperatures, owing to the non-negligible contribution of surface entropy. A higher degree of encapsulation can be obtained for larger Au NPs, because their higher surface energy facilitates their wetting by TiO₂⁵³.

An alternative strategy to enhance the hydrogenation activity of Au is based on the use of uniform Au NPs decorated with carbon atoms. Located in the interstitial positions in the lattice, carbon atoms can strongly affect the electronic properties of Au. The Au NP catalytic performance was investigated using synthesized Au interstitial nanocatalysts supported on ordered mesoporous carbonaceous materials and commercial catalysts (Au supported on SiO₂ and activated carbon)⁵⁵. The material with interstitial carbon species showed an improved catalytic performance and a high selectivity (well beyond 99%) compared with the commercial catalysts. To understand the observed catalytic trend, DFT and X-ray photoelectron spectroscopy studies were carried out. The presence of interstitial C enables the activation of H₂ molecules. Specifically, the electron transfer between C and Au leads to the heterolytic dissociation of H₂ on the C–Au interface. The unique adsorption configuration of C–Au further influences the chemisorption process due to its distinct electronic properties. This selective adsorption and activation of H₂ on Au surfaces containing interstitial C, as compared with pure surfaces, explains the

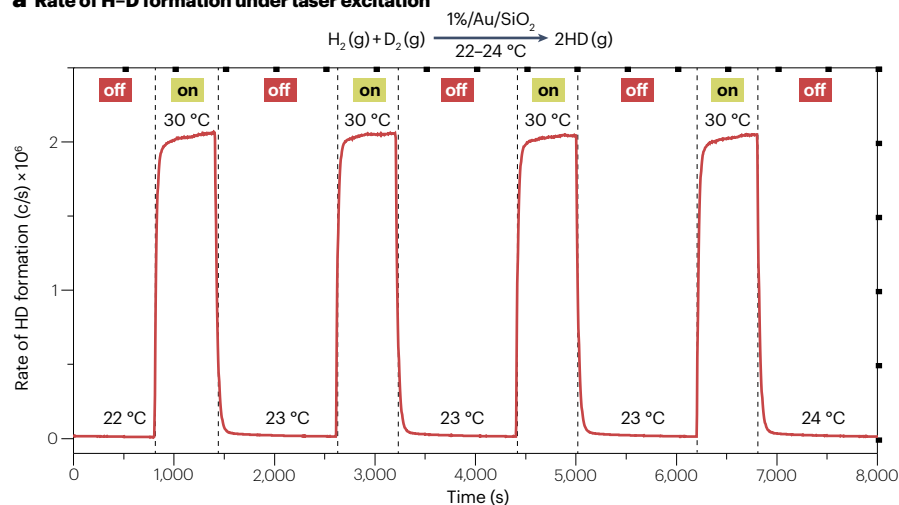
remarkable chemoselectivity observed for the Au interstitial nanocatalysts supported on ordered mesoporous carbonaceous materials when compared with commercial activated carbon supported Au NPs (Au/C) and Au/SiO₂ catalysts⁵⁵. Additionally, there may be a continuous exchange of C atoms between the surface and subsurface, potentially facilitating the adsorption of H₂ molecules. Moreover, in the case of the 3-nitrostyrene hydrogenation on Au supported mesoporous carbon catalysts, high chemoselectivity towards 3-vinylaniline was observed⁵⁵. This was attributed to the perpendicular adsorption of the substrate, stronger interaction of the 3-nitrostyrene with the C-containing Au surface and its enhanced activation on it. It was concluded that the high d-electron transfer from C to Au due to the C–Au interactions promotes the activation of 3-nitrostyrene on the C–Au interface. This enhanced H₂ dissociation improved the catalytic performance of the Au NPs in hydrogenation reactions⁵⁵.

Plasmon enhancement

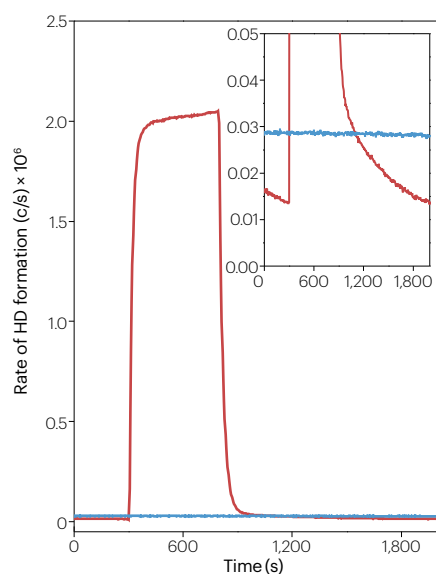
Taking advantage of the plasmonic properties of Au NPs, localized surface plasmon resonance (LSPR) is an alternative strategy to activate H₂^{21,40,56}. Here, hot electrons are formed from light illumination; these electrons then relax or scatter, initiating the catalytic hydrogenation reaction. Hot electrons are high-energy electrons produced through the interaction of light with metallic NPs or nanostructures, and they are being explored in new and exciting applications in nanotechnology and photonics. For catalysis, using hot electrons decreases the energy barrier for H–H activation owing to the transfer of electrons to the antibonding orbital of hydrogen⁴⁰.

Hot electrons induced the dissociation of hydrogen on small Au particles. When a Au NP is exposed to light with sufficient energy (for example visible light), absorbed photons excite electrons in the Au to higher energy levels. These hot electrons have excess energy compared with the equilibrium Fermi level of Au. This excess energy can be transferred to the hydrogen molecules and provide the activation energy required to activate them. Small Au supported on SiO₂ NPs prepared by chemical deposition precipitation method were used in H₂ dissociation experiments (Fig. 3). Figure 3a illustrates the rate of H–D formation on the Au/SiO₂ photocatalyst both with and without super-continuum laser excitation. Initially, the photocatalyst was maintained in the dark at 22–24 °C, yielding a constant background H–D level⁵⁶ (Fig. 3a). Upon laser activation, the rate of H–D generation immediately surged approximately 150-fold. This heightened rate stabilized within 10 minutes of laser stimulation. Concurrently, the sample's temperature rose by roughly 8 °C (up to 30 °C) due to laser-induced heating (Fig. 3a). After 10 minutes, the laser was deactivated, promptly restoring the system to its initial rate and temperature, showcasing the process's reversibility⁵⁶. For a direct comparison of H₂ dissociation efficiency between the Au/SiO₂ and Au/TiO₂ photocatalysts, Fig. 3b,c displays the monitored photocatalytic H–D formation rates for both catalysts. In contrast to the approximately 150-fold increase observed for Au/SiO₂ (Fig. 3b), the enhancement in the case of Au/TiO₂ (Fig. 3c) was modest, measuring around 2.7 times. The subdued rate for Au/TiO₂ may be attributed to the formation of a Schottky barrier (with a nominal height of 0.8–1 eV) at the Au–TiO₂ metal–semiconductor junction. During laser excitation, hot electrons possessing energies surpassing the barrier's height can effectively transfer from the Au NPs to TiO₂, contributing to the observed effects⁵⁶. The fact that the rate of hydrogen dissociation decreased substantially when SiO₂ was replaced by TiO₂, (Fig. 3b,c) indicates that H₂ dissociation occurring on the illuminated AuNP surface and the dielectric oxide is not participating

a Rate of H–D formation under laser excitation



b H–D formation rate for 1% Au/SiO₂ catalyst



c H–D formation rate for 1% Au/TiO₂ catalyst

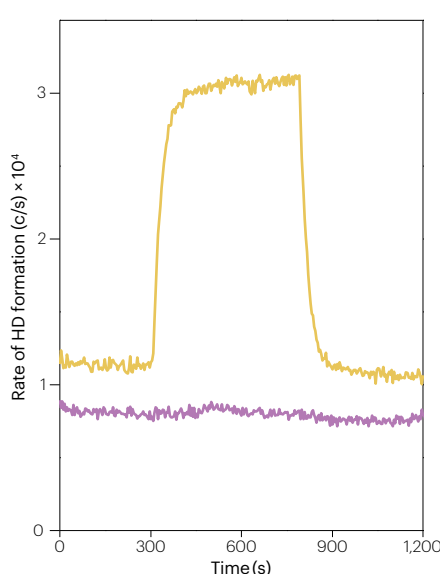


Fig. 3 | Hot electron-induced H–D formation at 23 °C on 1% Au/SiO₂ catalyst.

a, The rate of H–D formation was continuously monitored in real time under two conditions: with laser excitation (2.4 W cm^{-2} ; on) and without laser excitation (0.0 W cm^{-2} ; off). During the 10-minute period of laser excitation, the sample experienced a reversible temperature increase of $8\text{ }^\circ\text{C}$, as depicted in the figure, transitioning from 22 to $30\text{ }^\circ\text{C}$. **b**, H–D formation rate for the $1\% \text{ Au}/\text{SiO}_2$ catalyst. **c**, H–D formation rate for the $1\% \text{ Au}/\text{TiO}_2$ catalyst. With both catalysts, the same reaction conditions were applied: laser excitation of 2.4 W cm^{-2} (ref. 56). No activity was observed in the case of SiO_2 (blue curve) and TiO_2 (purple curve). The size of Au nanoparticles was $5\text{--}30\text{ nm}$, and the excitation wavelength ranged from 450 to $1,000\text{ nm}$. $1\% \text{ Au}/\text{SiO}_2$, 1 wt\% of Au on SiO_2 ; $1\% \text{ Au}/\text{TiO}_2$, 1 wt\% of Au on TiO_2 ; c/s, counts per second. Parts **a–c** adapted with permission from ref. 56, ACS.

in the process⁵⁶. A key challenge remains in the diffusion of hydrogen through the support and its recombination, which is essential to understanding the activity of hydrogen on a Au surface. The redshift in the LSPR of Au NPs is attributed to the charge transfer between Au and hydrogen atoms during hydrogen adsorption and diffusion. This charge transfer induces alterations in the properties of the Au NPs, causing a redshift in the LSPR. The observed red-shifted intensities are closely linked to variations in the sizes of the Au NPs, suggesting that hydrogen atoms predominantly adhere to specific facets or flat surfaces of the Au particles. H atoms may also recombine at this site and desorb into the gas phase again²¹. The measured LSPR shifts were of about 0.02 nm during H_2 adsorption (as measured by transmittance anisotropy spectroscopy)²¹. Hydrogen chemisorption occurred directly on Au. Furthermore, the relationship between the redshift intensity and the size of NPs indicates that dissociated hydrogen (H)

atoms migrate across the NP surfaces, predominantly on the (100) facets. These atoms subsequently recombine and desorb into the gas phase. Under an atmospheric pressure of H_2 , an average negative charge transfer of approximately -0.06 electron charge units from each surface Au atom to hydrogen (H) occurs, with a localized charge back-bonding estimated to be around -0.2 electron charge units for each Au–H bond. Consequently, these results confirmed, in line with theoretical studies, that, after H adsorption, the electron population in Au NPs decreases²¹. This enhanced comprehension of the chemisorption mechanism of H_2 onto Au NPs is anticipated to facilitate advancements in the fabrication and utilization of catalytic Au NPs for hydrogenation reactions²¹.

In photocatalytic reactions, Au NPs have exhibited unique catalytic properties, even at low temperatures or low light intensity. This suggests that the use of Au photocatalysts in chemical reactions governed

by mechanisms involving plasmonic effects and hot electron transfer may also be advantageous^{57–59}. This is especially true for hydrogenation reactions in which the hydrogen dissociation is often one of the limiting steps, as discussed above for the case of the photocatalytic hydrogen dissociation and H–D formation. The hot electrons transferred to H₂ were vital for the high yields, and the plasmon decay substantially lowered the energy barrier for hydrogen dissociation⁵⁶. Moreover, the dissociation of H₂ on the Au surface under visible-light excitation opens up the possibility for developing more efficient catalysts for the hydrogenation processes. For example, increased chemoselectivity was reported for the semi-hydrogenation of phenylacetylene under visible-light irradiation using a nanodesigned hybrid catalyst composed of a plasmonic core (Au or bimetallic Au@Ag) and Pt shells compared with classical SiO₂-supported Au catalysts⁶⁰.

To increase the catalytic performance of non-plasmonic metals like Pt, a successful integration of plasmonic and catalytic properties is required. The most widely used approach to achieve this is to harness the hot carriers generated through LSPR excitation. These hot carriers play a pivotal role in enhancing the catalytic activity of the material. Au/SiO₂ NPs and Au/TiO₂ NPs showed both negative (reduced reaction rate) and positive (catalytic enhancement) effects for 4-nitrophenol hydrogenation under visible-light illumination. The difference in plasmonic catalytic activities⁶¹ were attributed to the charge transfer at the interface of Au and the support as well as to the reducing agent (H₂ and NaBH₄) used during the catalyst synthesis. Au/SiO₂ NPs were substantially more active under plasmon excitation, whereas Au/TiO₂ catalysts were only enhanced by plasmons when H₂ (g) was used as the reducing agent. The decreased reaction rate observed upon reduction with BH₄[–] (aq.) was attributed to the transfer of hot electrons from Au to TiO₂.

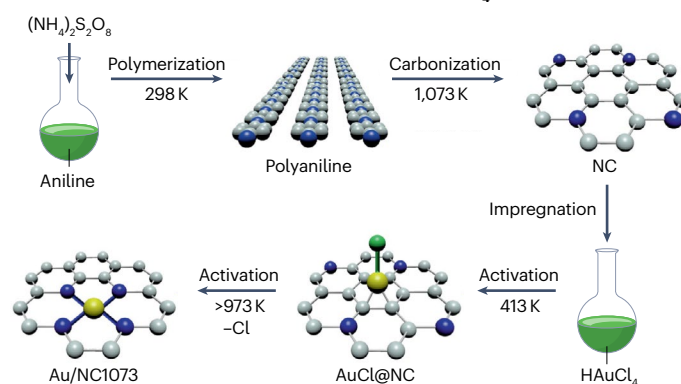
Cationic Au

An alternative approach to improving the activation of hydrogen is by using dispersed cationic Au species, in which isolated Au ions are dispersed throughout a carrier. The synthesis of these types of material is not trivial and usually requires several steps, as illustrated in Fig. 4a. In the case of Au supported on carbon nitride, the two most important steps are linked to the thermal treatment, first at low temperature (686 °C) and then at high temperature, above 1,246 °C (Fig. 4a). This structure resembles traditional organometallic catalysts^{62–67}, comprising isolated metals that are bound to organic ligands (Figs. 4b and 1e). These structures are also described as SACs, which are attracting increasing interest because they can make better use of the metal phase compared with standard metal NPs, and they have provided excellent levels of selectivity, activity and stability in hydrogenations^{68–72}. Cationic Au SACs decorated on multiwalled carbon nanotubes afforded a highly efficient hydrogenation of 1,3-butadiene and 1-butene under parahydrogen (an isomeric form of molecular hydrogen)⁷³. Atomically dispersed Au catalysts afforded better selectivity and activity in the pairwise addition of hydrogen than the supported Au NPs catalysts. Similarly, isolated Au species (Au⁺) supported on iron oxide (FeO_x) showed higher resistance to sintering (increase in particle size) than other Au nanostructures for alkene hydrogenations^{74–78}. Theoretical studies revealed that surface-anchored Au⁺ species exhibited very high stability and improved catalytic activity compared with other Au NP catalysts, because of the covalent Au–support interactions. For example, a supported Au(III) species anchored on a MgO surface induced high activity and selectivity in ethene hydrogenation⁷⁵. The conversion

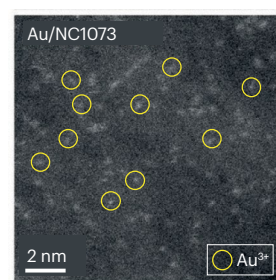
of ethene strongly depended on the Au–Au coordination number (Fig. 4c). The Au NPs were less efficient catalysts for ethene hydrogenation than Au SACs, and the atomic dispersion of the active phase (in SACs) was beneficial to drive the hydrogenation catalysis⁷⁵.

The developments in SAC design were made possible by advances in atomic-resolution microscopy that afford the imaging of the dispersed metal atoms and their evolution under reaction conditions^{79,80}. However, the practical use of Au SACs is often compromised by challenging synthesis protocols, which include the use of aqua regia as a dispersing agent, as well as the low resistance to sintering of non-functionalized carbon materials under reaction conditions³⁹. To address the difficulty of making such materials, a co-precipitation strategy can be implemented⁸¹. In it, the metal is added during synthesis of the metal–organic framework (MOF) precursors, intercalated

a Au(III)/NC synthesis and impregnation with HAuCl₄



b HAADF-STEM micrograph of Au/NC1073 catalyst (Au SACs circled)



c Ethene hydrogenation turnover frequency

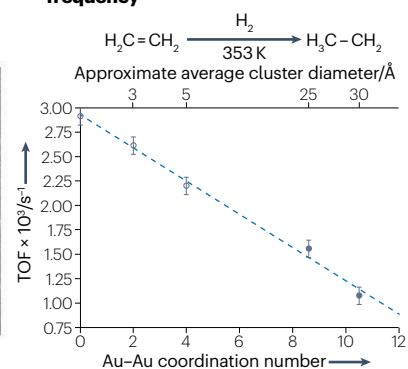


Fig. 4 | Au single-atom catalysts. **a**, Schematic representation of the nitrogen-doped carbon (Au(III)/NC) synthesis and impregnation with HAuCl₄ used as Au precursor. Impregnation step performed via incipient wetness impregnation of nitrogen-doped carbon (NC) with HAuCl₄ in aqua regia solution. Two thermal treatments were applied: activation step in static air (at 473 K) and flowing N₂ (>973 K) for 16 h. Colour coding: Au, yellow; C, grey; N, blue; Cl, green⁴¹. **b**, Aberration-corrected high-angle annular dark-field scanning transmission electron microscopy (HAADF-STEM) micrographs of Au/NC1073 catalyst with Au single-atoms catalysts (SACs) circled (scale bar: 2 nm)⁴¹. **c**, Turnover frequency (TOF) of ethene hydrogenation as a function of the single Au–Au coordination number on different MgO-supported catalysts containing Au³⁺ and Au clusters⁷⁵. Part **a** reprinted with permission from ref. 41, Wiley. Part **b** adapted with permission from ref. 41, Wiley. Part **c** reprinted with permission from ref. 75, Wiley.

Box 3

Bimetallic synergy

Bimetallic synergy can substantially improve the catalytic properties of a monometallic catalyst and can even promote new catalytic abilities that are not possible for a monometallic catalyst. The addition of a second metal can alter the activity, selectivity and resistance to deactivation inherent to the monometallic particles. The structures of bimetallic particles differ from those of bulk alloys, and they are categorized into core-shell, mixed and Janus structures (examples of different structures are provided in the figure below; STEM, scanning transmission electron microscopy; SEM, scanning electron microscopy); the said structures are mainly determined by the nature of the metal, the molar ratio between the metals and the method used for their synthesis¹¹¹. Bimetallic nanoparticles can experience surface segregation phenomena (distribution of the two different metals on the surface of the nanoparticle is not homogeneous, and one of the metals tends to concentrate or segregate on the surface), which are crucial in both the synthesis and applications of these nanoparticles. Au-based bimetallic catalysts have been studied in hydrogenation reactions; the most common among them are Au–Pt^{24,112}, Au–Pd^{92,93,101,102,113}, Au–Ir¹¹⁴, Au–Ag¹¹⁵, Au–Cu¹¹⁶, Au–Ni¹⁰⁰ and Au–SiO₂¹¹⁷.

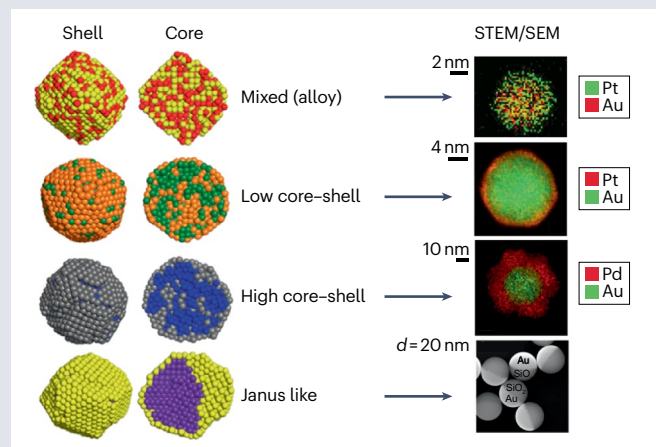


Figure (left) is adapted from ref. 111, CC BY 4.0. Right, second from top, adapted from ref. 112, Springer Nature Limited. Right, third from top, adapted from ref. 113, Springer Nature Limited. Right, bottom, adapted from ref. 117, Springer Nature Limited.

through the layers via electrostatic surface interactions replacing anions present in the MOF structures (for example, the sulfate ion). The positively charged Au atoms were detected using high-angle annular dark-field scanning transmission electron microscopy imaging and extended X-ray absorption fine structure measurements. This approach is analogous to the copolymerization route used for the immobilization of isolated atoms on graphitic C₃N₄^{82,83}. Au SACs prepared by co-precipitation methods were tested in the hydrogenation of *p*-nitrophenol to *p*-aminophenol and showed improved activity compared with classically prepared MOFs⁸¹. In addition, after ten

catalytic cycles, the catalyst retained its original morphology and activity, indicating excellent stability⁸¹.

A kg-scale synthesis of Au₁/CeO₂ SAC was reported implementing a dry ball milling synthetic protocol⁸⁴. This catalyst was then tested in the hydrogen oxidation (1 vol% H₂ + 1 vol% O₂ balanced with He). The catalyst afforded only ~10% hydrogen conversion at 160 °C⁸⁴. Despite a modest yield, this approach is a proof-of-concept that noble metal supported SACs can be prepared in large scale using a facile and reproducible methodology.

Alloying and bimetallic synergy

Hydrogen dissociation can also be improved by taking advantage of Au alloying to generate weakly bound H atoms^{85–87}. Ideally, an alloy structure (Box 3) should effectively combine one metal (Pt-group metals, and metals in the Pd and Pt triads especially) that promotes hydrogen dissociation and another (Au, Cu or Ag) that can react with the dissociated H atoms and thus promote hydrogenation^{88,89}. The most promising bimetallic catalysts for processes involving hydrogen are Au–Pd NPs in either an alloy in which the two different metals are homogeneously arranged or in a core-shell structure in which one metal is in the core and the second metal forms the shell⁹⁰. The optimal ensemble configuration for heterolytic H₂ activation remains up for debate. In Au–Pd alloys with a controlled density of Pd atom ensembles on the surface (monomers, dimers and trimers) the presence of neighbouring Pd atoms is crucial for hydrogen activation. In other words, the ensemble must be at least a dimer, as Pd monomers are not able to adsorb hydrogen⁹¹.

It is important to identify the sites responsible for the activation of H₂ in Au–Pd alloyed systems. Not only does this facilitate the identification of the minimal Pd ensemble (quantity of Pd needed to catalyse a reaction with optimal efficiency) for the activation of H₂, but it also reveals the energy profile for the spillover and release of hydrogen. The hydrogen spillover effect is an interfacial phenomenon in which active H atoms generated by the dissociation of H₂ on one phase (metal surface) migrate to another phase (support surface) and participate in the catalytic reaction of the substance adsorbed on that site. By modelling Au–Pd systems, it was anticipated that Pd atoms in a (111) surface of Au could activate H₂⁹². By combining temperature programmed desorption and high-resolution scanning transmission electron microscopy, it was shown that a low number of isolated atoms of Pd are responsible for hydrogen dissociation. The quantity of surface atoms of Pd in Au reflects the number of H atoms adsorbed on the surface. Further temperature programmed desorption–H–D exchange and DFT studies provided the energetic landscape for the adsorption of H₂, including an understanding of the activation and desorption of hydrogen from isolated Pd atoms, the typical reaction pathway for activating H₂ and the mechanism of the release of hydrogen along the Pd atoms with minimum spillover of hydrogen species to the Au⁹³.

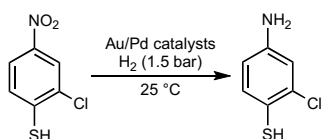
Using spatially resolved tip-enhanced Raman spectroscopy^{94–96}, a study of the catalytic hydrogenation of chloronitrobenzenethiol to chloroaminobenzenethiol (Fig. 5a) over Au–Pd catalyst was carried out⁹⁶ (Fig. 5a–f). Tip-enhanced Raman spectroscopy provides information on the topography and chemical composition of a surface with high accuracy and at the excellent resolution of ~10 nm. To gain a more comprehensive understanding of the chloronitrobenzenethiol hydrogenation process, a quantitative characterization of the relationship between the active regions (blue regions in Fig. 5c,e) and surface structures was conducted⁹⁶. In Fig. 5d,f, two distinct regions, each measuring 100 nm in width, featuring Pd islands (Fig. 5d) and

Au craters (Fig. 5f) in the tip-enhanced Raman spectroscopy maps, are represented. Co-localized scanning tunnelling microscopy images with accompanying height profiles are also given (as inserts in Fig. 5d,f). In these representations, the active region is highlighted in light blue whereas the non-reactive region is depicted in light red. In the case of Pd_{LC}/Au (Au surface with low Pd coverage; Fig. 5c,d), the size of the active regions, is approximately 50 nm⁹⁶. However, the size of the Pd islands within both regions is only 20 nm. Conversely, for Pd_{HC}/Au (Au surface with high Pd coverage; Fig. 5e,f), the active regions are approximately 15 nm larger than the Pd layer itself. The results reveal that the active regions extend approximately 15–30 nm beyond the boundaries of the Pd areas, where hydrogenation reactions occur. These spillover regions, however, exhibit an asymmetrical relationship with the shape of the Pd islands⁹⁶ (Fig. 5c). The obtained results

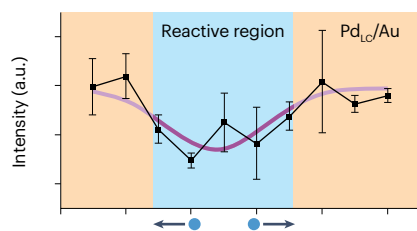
revealed that hydrogenation takes place beyond the Pd active sites and was initiated by the spilt-over hydrogen dissociated on Pd. After dissociation on Pd, hydrogen atoms migrated to adjacent Au surfaces over the relatively long distance of 15–30 nm⁹⁶. The mechanism of this hydrogenation involving hydrogen spillover was also determined by DFT; this evidence confirmed the feasibility of the long-distance diffusion and explained the enhanced chemoselectivity towards the reactant in the Au–Pd bimetallic catalyst.

Single-atom alloys (SAAs) are a class of single-site catalysts in which small amounts of isolated metal atoms are present in the surface layer of a metal that plays the role of the host^{88,89,97,98}. Typically, SAAs are comprised of single atoms of a catalytically active metal alloyed into the surface of a less reactive host metal. For example, for the hydrogenation of butadiene to butene, hydrogen is dissociated

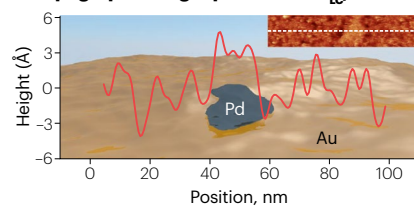
a Catalytic hydrogenation of chloronitrobenzenethiol to chloroaminobenzenethiol



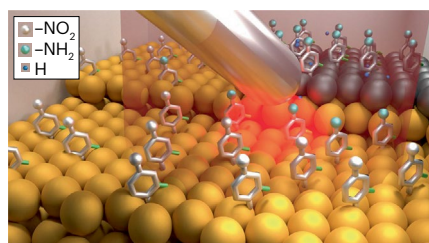
c NO₂ stretching bond (Raman) intensity in TERS line scan spectra on Pd_{LC}/Au



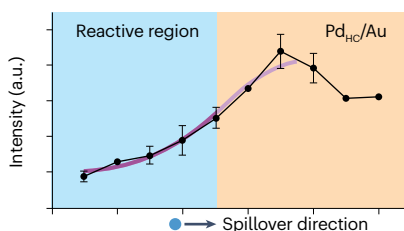
d Topographic height profile for Pd_{LC}/Au



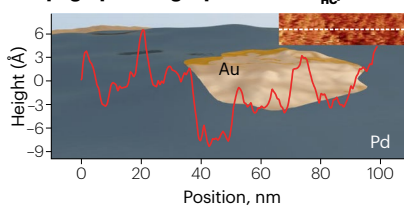
b STM-TERS illustration of an Ag tip investigating hydrogenation on Au–Pd



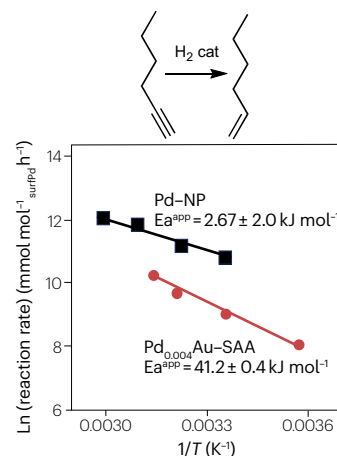
e NO₂ stretching bond (Raman) intensity in TERS line scan spectra on Pd_{HC}/Au



f Topographic height profile for Pd_{HC}/Au



g Reaction rate for time-resolved hydrogenation of 1-hexyne over PdAu-SAA/SiO₂ vs monometallic Pd/SiO₂



h Selectivity profile

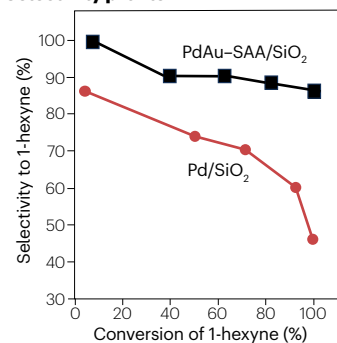
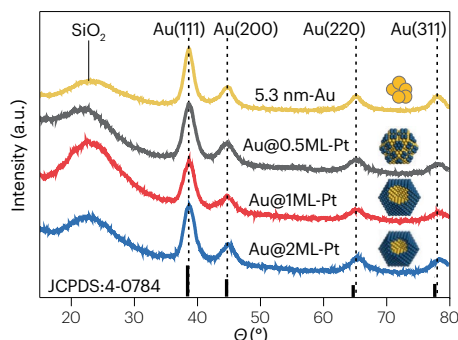


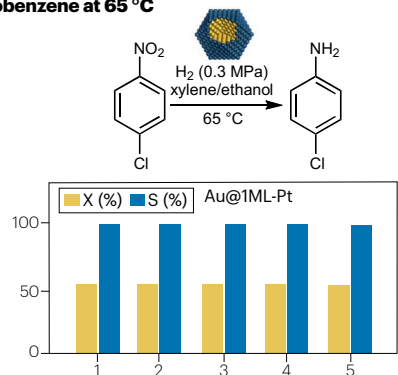
Fig. 5 | Spillover region identification. **a**, Reaction scheme of the catalytic hydrogenation of chloronitrobenzenethiol to chloroaminobenzenethiol on Au–Pd bimetallic catalysts at 25 °C. **b**, Illustration of scanning tunnelling microscopy coupled with tip-enhanced Raman spectroscopy (STM-TERS) utilizing an Ag tip to investigate hydrogenation products on a Pd–Au bimetallic substrate. The grey hexatomic rings represent benzene rings; the small blue spheres represent hydrogen. **c**, Intensity of the peak at 1,336 cm⁻¹ (NO₂ stretching bond in Raman spectra) in TERS line scan spectra on low Pd coverage on Au surface (Pd_{LC}/Au). The size of the active region is represented by the blue regions. Blue arrows accompanied by dots indicate the hydrogen spillover direction⁹⁶. **d**, Topographic height profile for Pd_{LC}/Au (indicated by the red line) of the surface along the dashed line in the inset of the respective STM images is

overlaid with a schematic of the surface structure. In this representation, Au is depicted in yellow shading whereas Pd is depicted in grey shading. **e**, Intensity of the peak at 1,336 cm⁻¹ in TERS line scan spectra on high Pd coverage on Au surface (Pd_{HC}/Au). The blue arrow accompanied by a dot indicates the hydrogen spillover direction. **f**, Topographic height profile of Pd_{HC}/Au. **g** and **h**, Reaction rate and selectivity profiles of time-resolved hydrogenation of 1-hexyne over PdAu-SAA/SiO₂ catalysts compared with monometallic Pd/SiO₂ catalyst, respectively. cat, catalyst; Ea^{app}, apparent activation energy; Pd–NP, Pd/SiO₂ catalyst; Pd_{0.004}Au–SAA, Pd–Au single atom alloy. Parts **b–f** reprinted from ref. 96, Springer Nature Limited. Part **g** adapted with permission from ref. 98, ACS. Part **h** reprinted with permission from ref. 98, ACS.

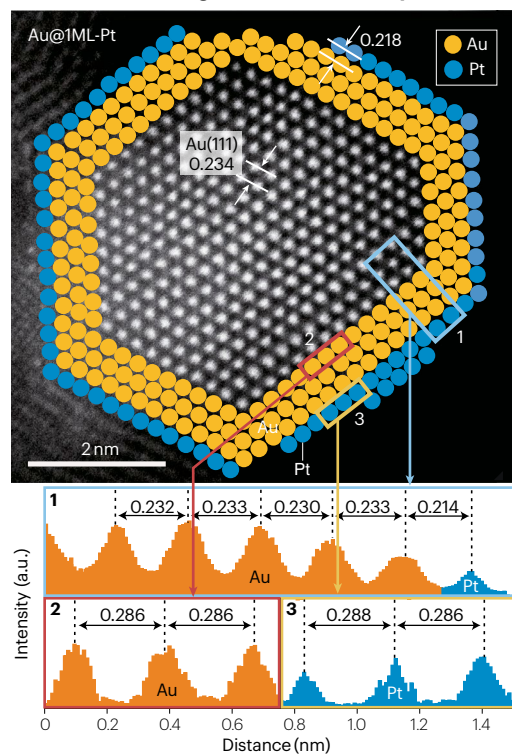
a X-ray diffractometry patterns of monometallic Au and bimetallic Au@Pt systems



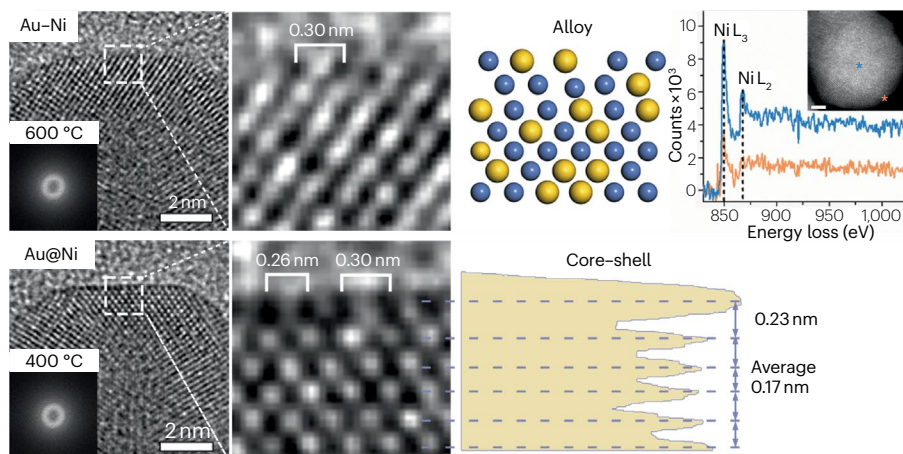
b Recycling of Au@ML-Pt catalyst in hydrogenation of chloronitrobenzene at 65 °C



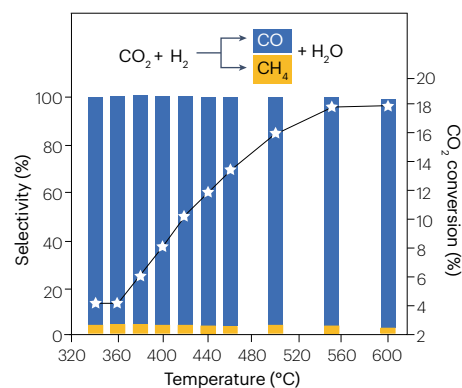
c HAADF-STEM image of Au@1ML-Pt catalyst



d Surface atom arrangement in Au-Ni bimetallic nanoparticle at 600 °C and 400 °C



e Selectivity and conversion profiles for the Au-Ni bimetallic catalyst



f Energy routes for CO₂ hydrogenation on the alloyed Au-Ni surface

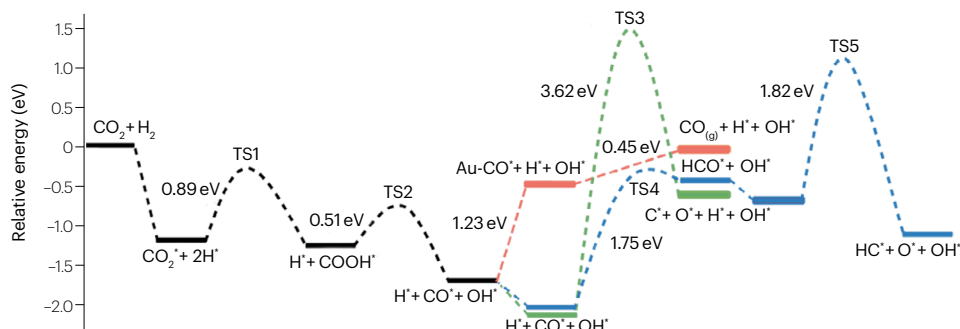


Fig. 6 | Morphology in the structure of the bimetallic Au@Pt core-shell nanocatalyst. **a**, X-ray diffractometry patterns of monometallic Au and bimetallic Au@Pt (core-shell structure) systems. The structure of the Au core is preserved after Pt shell formation, as determined based on the diffraction peaks of Au from the JCPDS-4-0784 database. **b**, Recycling tests for the Au@IML-Pt catalyst in the chemoselective hydrogenation of chloronitrobenzene at 65 °C. The activity of the catalyst is stable over five cycles. X (%), chloronitrobenzene conversion; S (%), selectivity to *para*-chloroaniline. **c**, High-angle annular dark-field scanning transmission electron microscopy (HAADF-STEM) image of Au@IML-Pt catalyst accompanied by the corresponding line intensity profiles along the numbered coloured rectangles. These profiles reveal both the interplanar distance and the lattice distance. As depicted in the figure, yellow and blue spheres correspond to the Au core and blue ones to the Pt shell. **d**, Surface atom arrangement in Au–Ni bimetallic nanoparticle at 600 °C (top image) and at 400 °C (bottom image). After thermal treatment at 600 °C, the alloy structure is formed between Ni and Au. Once the temperature decreases to

400 °C, dealloying takes place, and the core-structure is formed. The formation of an alloy at 600 °C is responsible for the high selectivity of this catalyst in CO₂ hydrogenations showed in Fig. 6e. On the right a point analysis of the electron energy loss spectra (with a HAADF inset) is presented. Blue and orange curves correspond to the points analysed as shown in the HAADF inset. **e**, Selectivity and conversion temperature resolved profiles for the Ni–Au bimetallic catalyst. The highest conversion is obtained at 600 °C, at which temperature the alloy structure is formed. **f**, Energy routes for the CO₂ hydrogenation reaction on the (111) surface of the alloyed Ni–Au phase are depicted. The alloying process and reaction pathways are elucidated through density functional theory calculations and Fourier-transform infrared spectroscopy experiments, shedding light on the mechanism. TS, transition state. Part **a** adapted from ref. 24, Springer Nature Limited. Part **c** reprinted from ref. 24, Springer Nature Limited. Parts **e** and **f** reprinted from ref. 100, Springer Nature Limited. Part **d** adapted from ref. 100, Springer Nature Limited.

at isolated metal sites, for example Pt, and the hydrogen atoms spill over onto the host metal, such as Cu, where the reactant (butadiene) reacts to form the product (butene). This species then desorbs prior to complete hydrogenation, demonstrating the chemoselectivity of this catalyst⁸⁹. Such materials have also attracted interest owing to their potential to break linear scaling relationships in alloy catalysis. Under standard conditions (low temperature) Au is not able to activate hydrogen; however, using SAAs of Au, highly selective hydrogenation reactions are enabled, such as the selective hydrogenation of 1-hexene to 1-hexene using Au–Pd SAA catalyst (Fig. 5g,h). The facile activation of hydrogen on Pd is possible using Au–Pd SAAs in which Au is incapable of dissociating molecular hydrogen⁹⁸. To overcome this limitation, addition of small amounts of Pd to form a Au–Pd SAA has been reported to activate molecular hydrogen, although the dissociated hydrogen does not spill over onto the Au host⁹⁷. In operando spectroscopy studies confirmed that the transformation occurs by first dissociating H₂ and splitting of the hydrogen species on the Pd sites followed by the reaction of the adsorbed H species on Au⁹⁷. Moreover, by conducting DFT studies on the Pd–Au(111) surface, it was shown that the C atom is bound to the Pd atom. Because the H atom is also bound more strongly to the Pd atom, it is more kinetically favourable to hydrogenate this mid-compound C atom than a terminal C atom. This considerably limits over-hydrogenation and oligomerization side reactions.

In bimetallic NPs, the chemical composition and order affect the catalytic properties of bimetallic systems⁹⁹. The incorporation of a second metal can help overcome the limitations observed for monometallic NPs, such as redox properties, stability, substrate adsorption and decrease in activity when NP size increases. DFT predicted that by overcoming the size-dependent correlation observed on monometallic Pt catalysts in this reaction, a monolayer of Pt and Au catalyst would lead to higher activity as well as higher chemoselectivity in the hydrogenation of halonitrobenzenes²⁴. As such, an Au@Pt/SiO₂ catalyst with core(Au)–shell(Pt) structure supported on SiO₂ and with a monolayer Pt shell was prepared using the atomic layer deposition methodology. In addition, the catalytic activity of a range of bimetallic Au–Pt catalysts using 0.5, 1 and 2 monolayer Pt shells, with 1 monolayer of Pt shell (Fig. 6a) were compared in terms of the selectivity towards *para*-chloroaniline²⁴ (Fig. 6b). The core-shell structure was confirmed using high-resolution microscopy (Fig. 6c), and such data revealed a Pt shell thickness of about 0.3 nm (blue line in Fig. 6c) in the case of the Au@IML-Pt catalyst (core-shell structure with 1 monolayer of Pt

on Au core supported on SiO₂). The Au@IML-Pt catalyst exhibited a high catalytic activity (Fig. 6b) owing to the enhanced charge transfer between Au and Pt atoms facilitated by the substantial ligand effect. The ligand effect can have a profound impact on the catalytic activity and specificity of the catalyst, as the ligands can bind to the metal surface and significantly modify its electronic and steric properties. The DFT studies also confirmed that the terrace sites responsible for high selectivity were preserved²⁴, which increases the stability of the catalyst. These flat NP surface regions with regularly arranged atoms play a vital role in catalysis by providing stable and well-defined surfaces for chemical reactions. Finally, the catalyst presented high stability compared with the monometallic Pt catalyst, which generally suffers from the agglomeration and leaching of Pt particles and from chlorine poisoning²⁴.

Au-based bimetallic catalysts were also shown to exhibit excellent CO₂ hydrogenation activity, forming CO. For example, Ni–Au bimetallic catalytic systems based on core-shell structure are very active for this reaction¹⁰⁰ (Fig. 6d). SiO₂ was chosen as a support of the core-shell NPs, which consisted of a face-centred cubic (fcc structure, in which atoms are arranged at the corners and centre of each cube face of the cell) Ni core, and a Au shell formed by 2–3 atomic layers (Fig. 6d). Catalytic studies showed the Ni–Au bimetallic catalyst provided a high selectivity towards CO (95%), with a conversion rate of 4.5–18% in the 340–600 °C temperature range¹⁰⁰ (Fig. 6e). Ex situ scanning transmission electron microscopy characterization showed the presence of a core-shell structure, with an ultrathin Au shell. However, during in situ scanning transmission electron microscopy imaging, a phase transition was observed with the creation of a new Au–Ni alloy phase at similar reaction temperatures. In addition, in situ transmission electron microscopy analysis revealed that, during the heat treatment from 450 to 600 °C, the Au species at the outmost surface were dissolved in the Ni matrix forming an alloy¹⁰⁰ (Fig. 6d, top section). However, during the cooling process back to 450 °C, a dealloying process occurred, and the Ni@Au core-shell structure was recovered (Fig. 6d, bottom section). Control experiments carried out in a gas-cell reactor minimized the ‘pressure gap’ observed between the in situ environmental transmission electron microscopy measurements (–9 mbar) and the actual reaction conditions (1 bar) and reproduced the reaction-driven alloying of Au–Ni NPs, which confirmed the credibility of their original transmission electron microscopy results. Finally, DFT calculations confirmed the identity of the most energetically favoured reaction pathway, which consisted

of two stages. The first was CO₂ hydrogenation to form adsorbed CO, and the second was the diffusion of CO adsorbed on Ni to the Au sites, finally leading to the desorption of CO (Fig. 6f). These results confirmed that the Ni active sites were responsible for the CO₂ hydrogenation and the Au active sites for the high-selectivity CO formation¹⁰⁰. These results confirmed that the alloying–dealloying mechanism took place in the bimetallic Au–Ni systems. This is also the case for Au–Pd alloys. Pretreatment in oxygen leads to an enhancement in the activity in dilute Au–Pd alloys by bringing Pd to the surface of the Au particle. On the contrary, during the hydrogen treatment, the Pd returns to the bulk and the catalyst undergoes deactivation^{101,102}.

Conclusion and outlook

Au-based nanomaterials remain promising catalysts for selective hydrogenation reactions. The hydrogen activation pathway can be promoted in catalytic hydrogenations in four ways: assistance from light, the size of the metal NPs, the Au–support interaction, and the presence of ligands or modifiers on the metal surface. Additionally, exploring the two activation modes (homolytic scission to H atoms or heterolytic scission into H⁺/H⁻ pairs) in turn can make these catalytic processes more efficient. For example, to perform selective hydrogenations, organic linkers must be present on the Au surface to promote heterolytic scission.

Two key challenges in the development of Au-based nanomaterials for hydrogenation catalysts are the need to control the sintering of the Au species during the reaction and the low solvent tolerance of these catalysts. Research continues in the search for appropriate promoters and components that are able to enhance the catalytic activity of supported Au catalysts. The choice of the promoter depends on the specific catalytic reaction and the desired enhancement in catalytic properties. Promoters play a crucial role in tailoring the activity, selectivity and stability of Au NPs for various applications in catalysis. Some of the most important promoters are organic ligands, sulfur-containing species, metals and oxides (especially for core–shell structures). Moreover, shifting from neutral Au NPs to cationic Au single atoms appears to improve the catalysts' durability and open new pathways for catalyst regeneration¹⁰³.

Another important challenge will be the use of hybrid catalysts mixing single atoms and nanoscale particles^{104–106}. In this case, cascade reactions may be performed or the reaction rate can be substantially improved. The use of hybrid mixtures (SACs + NPs) could be a useful parameter to explore in reactions involving hydrogen, as hydrogen dissociation and reactivity strongly depend on the size of the Au particle.

Finally, we need an improved fundamental understanding of the hydrogenation mechanisms, as it should provide useful information for the rational design of new Au catalysts. To better understand the catalyst reduction process and the nature and formation of intermediates, advanced in situ characterization techniques will be required. The main issues are still linked to the very small size of active Au species. The use of synchrotron facilities is required to fully characterize these materials. However, these facilities are in high demand among researchers from various scientific disciplines, including physics, chemistry and materials science. In situ techniques are also challenging, as very often the relevant experiments require extended setup and data collection times owing to their complexity. A crucial factor often neglected is also the very first atomic layer in the case of bimetallic NPs. Probing the core and surface composition of nanoalloys to rationalize their selectivity is of high importance for understanding their catalytic selectivity. A characterization methodology must be developed to distinguish between the surface and core composition. Identification of the optimal balance

between the two metals will help tune the relative rates of various reaction pathways and, consequently, control the selectivity of the catalytic process. A combination of experimental analysis and DFT simulations will also be required to understand the adsorption–desorption process and the selectivity path to a specific product.

In summary, by adopting a multidisciplinary approach (material sciences, physics, chemistry, biology and engineering), as well as by leveraging advanced characterization and computational methods, researchers can explore future applications of Au-based materials. The integration of advanced characterization techniques and computational methods enhances our understanding and paves the way for new advances. Au-based materials, when viewed through this multidisciplinary lens, hold immense promise, not only in hydrogenation processes but also in other domains. Beyond their traditional roles, these materials have emerged as catalysts in the realm of sensing technologies, affording novel possibilities for detecting and responding to various stimuli. Moreover, in the field of nanomedicine, Au-based materials may contribute to advances in diagnostics and therapies. As nanocarriers, they have the potential to stand at the forefront of innovative drug delivery systems, offering tailored solutions for precision medicine and revolutionizing the landscape of therapeutic interventions. Au-based materials are poised to be versatile tools across a spectrum of applications that transcend disciplinary boundaries.

Published online: 23 February 2024

References

- Wood, B. & Wise, H. The role of adsorbed hydrogen in the catalytic hydrogenation of cyclohexene. *J. Catal.* **5**, 135–145 (1966).
- Fujitani, T., Nakamura, I., Akita, T., Okamura, M. & Haruta, M. Hydrogen dissociation by gold clusters. *Angew. Chem. Int. Ed.* **48**, 9515–9518 (2009).
- Vogt, C. & Weckhuysen, B. M. The concept of active site in heterogeneous catalysis. *Nat. Rev. Chem.* **6**, 89–111 (2022).
- Navarro-Jaén, S. et al. Highlights and challenges in the selective reduction of carbon dioxide to methanol. *Nat. Rev. Chem.* **5**, 564–579 (2021).
- Shuo, C., Wojcieszak, R., Dumeignil, F., Marceau, E. & Royer, S. How catalysts and experimental conditions determine the selective hydroconversion of furfural and 5-hydroxymethylfurfural. *Chem. Rev.* **118**, 11023–11117 (2018).
- Zugic, B. et al. Dynamic restructuring drives catalytic activity on nanoporous gold–silver alloy catalysts. *Nat. Mater.* **16**, 558–564 (2017).
- Hvolbæk, B. et al. Catalytic activity of Au nanoparticles. *Nano Today* **2**, 14–18 (2007).
- Fujita, T. et al. Atomic origins of the high catalytic activity of nanoporous gold. *Nat. Mater.* **11**, 775–780 (2012).
- Wang, H. et al. Strong metal–support interactions on gold nanoparticle catalysts achieved through Le Chatelier's principle. *Nat. Catal.* **4**, 418–424 (2021).
- Lopez, N. et al. On the origin of the catalytic activity of gold nanoparticles for low-temperature CO oxidation. *J. Catal.* **223**, 232–235 (2004).
- Qian, H., Zhu, M., Wu, Z. & Jin, R. Quantum sized gold nanoclusters with atomic precision. *Acc. Chem. Res.* **45**, 1470–1479 (2012).
- Haruta, M. When gold is not noble: catalysis by nanoparticles. *Chem. Rec.* **3**, 75–87 (2003).
- Corma, A. & Garcia, H. Supported gold nanoparticles as catalysts for organic reactions. *Chem. Soc. Rev.* **37**, 2096–2126 (2008).
- Bond, G. C. Hydrogenation by gold catalysts: an unexpected discovery and a current assessment. *Gold Bull.* **49**, 53–61 (2016).
- Delgado, J. A. & Godard, C. in *Recent Advances in Nanoparticle Catalysis. Molecular Catalysis*, Vol. 1 (eds Van Leeuwen, P. W. N. M. & Claver, C.) 303–344 (Springer, Cham, 2020).
- Hutchings, G. Heterogeneous gold catalysis. *ACS Cent. Sci.* **4**, 1095–1101 (2018).
- Bus, E., Miller, J. T. & van Bokhoven, J. A. Hydrogen chemisorption on Al₂O₃-supported gold catalysts. *J. Phys. Chem. B* **109**, 14581–14587 (2005).
- Green, I. X., Tang, W., Neurock, M. & Yates, J. T. Low-temperature catalytic H₂ oxidation over Au nanoparticle/TiO₂ dual perimeter sites. *Angew. Chem. Int. Ed.* **50**, 10186–10189 (2011).
- Manzoli, M., Chiorino, A., Vindigni, F. & Boccuzzi, F. Hydrogen interaction with gold nanoparticles and clusters supported on different oxides: a FTIR study. *Catal. Today* **181**, 62–67 (2012).
- Boronat, M., Concepcion, P. & Corma, A. Unravelling the nature of gold surface sites by combining IR spectroscopy and DFT calculations. implications in catalysis. *J. Phys. Chem. C* **113**, 16772–16784 (2009).

21. Watkins, W. L. & Borenstein, Y. Mechanism of hydrogen adsorption on gold nanoparticles and charge transfer probed by anisotropic surface plasmon resonance. *Phys. Chem. Chem. Phys.* **19**, 27397–27405 (2017).
22. Hammer, B. & Norskov, J. K. Why gold is the noblest of all the metals. *Nature* **376**, 238–240 (1995).
23. Sun, X. et al. Facile synthesis of precious-metal single-site catalysts using organic solvents. *Nat. Chem.* **12**, 560–567 (2020).
24. Guan, Q. et al. Bimetallic monolayer catalyst breaks the activity–selectivity trade-off on metal particle size for efficient chemoselective hydrogenations. *Nat. Catal.* **4**, 840–849 (2021).
25. Chmielewski, A. et al. Reshaping dynamics of gold nanoparticles under H₂ and O₂ at atmospheric pressure. *ACS Nano* **13**, 2024–2033 (2019).
26. Bai, S. T. et al. Homogeneous and heterogeneous catalysts for hydrogenation of CO₂ to methanol under mild conditions. *Chem. Soc. Rev.* **50**, 4259–4298 (2021).
27. Gesesse, D. et al. A soft-chemistry assisted strong metal–support interaction on a designed plasmonic core–shell photocatalyst for enhanced photocatalytic hydrogen production. *Nanoscale* **12**, 7011–7023 (2020).
28. Ferraz P, C. et al. Enhancing the activity of gold supported catalysts by oxide coating: towards efficient oxidations. *Green Chem.* **23**, 8453–8457 (2021).
29. Nguyen, K. T. et al. Unusual hydrogen implanted gold with lattice contraction at increased hydrogen content. *Nat. Commun.* **12**, 1560 (2021).
30. Martin, A. J., Mitchell, S., Mondelli, C., Jaydev, S. & Pérez-Ramirez, J. Unifying views on catalyst deactivation. *Nat. Catal.* **5**, 854–866 (2022).
31. Segura, Y., Lopez, N. & Perez-Ramirez, J. Origin of the superior hydrogenation selectivity of gold nanoparticles in alkyne + alkene mixtures: triple- versus double-bond activation. *J. Catal.* **247**, 383–386 (2007).
32. van Deelen, T. W., Hernández Mejía, C. & de Jong, K. P. Control of metal-support interactions in heterogeneous catalysts to enhance activity and selectivity. *Nat. Catal.* **2**, 955–970 (2019).
33. Vijay, S. et al. Unified mechanistic understanding of CO₂ reduction to CO on transition metal and single atom catalysts. *Nat. Catal.* **4**, 1024–1031 (2021).
34. Norskov, J., Bligaard, T., Rossmeisl, J. & Christensen, C. H. Towards the computational design of solid catalysts. *Nat. Chem.* **1**, 37–46 (2009).
35. Milone, C. et al. Selective hydrogenation of α,β -unsaturated ketones to α,β -unsaturated alcohols on gold-supported catalysts. *J. Catal.* **222**, 348–356 (2004).
36. Silva, R., Fiorio, J., Vidinha, P. & Rossi, L. M. Gold catalysis for selective hydrogenation of aldehydes and valorization of bio-based chemical building blocks. *J. Braz. Chem. Soc.* **30**, 2162–2169 (2019).
37. Fiorio, J. & Rossi, L. Clean protocol for deoxygenation of epoxides to alkenes via catalytic hydrogenation using Au. *Catal. Sci. Technol.* **11**, 312–318 (2021).
38. Fiorio, J., Lopez, N. & Rossi, L. Gold–ligand-catalyzed selective hydrogenation of alkynes into *cis*-alkenes via H₂ heterolytic activation by frustrated Lewis pairs. *ACS Catal.* **7**, 2973–2980 (2017).
39. Whittaker, T. et al. H₂ oxidation over supported Au nanoparticle catalysts: evidence for heterolytic H₂ activation at the metal–support interface. *J. Am. Chem. Soc.* **140**, 16469–16487 (2018).
40. Mukherjee, S. et al. Hot electrons do the impossible: plasmon-induced dissociation of H₂ on Au. *Nano Lett.* **13**, 240–247 (2013).
41. Lin, R. et al. Design of single Au atoms on nitrogen-doped carbon for molecular recognition in alkyne semi-hydrogenation. *Angew. Chem. Int. Ed.* **58**, 504–509 (2019).
42. Stephan, D. W. The broadening reach of frustrated Lewis pair chemistry. *Science* **354**, aaf7229 (2016).
43. Fiorio, J. et al. Accessing frustrated Lewis pair chemistry through robust Au@N-doped carbon for selective hydrogenation of alkynes. *ACS Catal.* **8**, 3516–3524 (2018).
44. Lu, C. et al. Gold catalyzed hydrogenations of small imines and nitriles: enhanced reactivity of Au surface toward H₂ via collaboration with a Lewis base. *Chem. Sci.* **5**, 1082–1090 (2014).
45. Almora-Barrios, N., Cano, I., van Leeuwen, P. & Lopez, N. Concerted chemoselective hydrogenation of acrolein on secondary phosphine oxide decorated gold nanoparticles. *ACS Catal.* **7**, 3949–3954 (2017).
46. Lv, X., Lu, G., Wang, Z.-Q., Xu, Z.-N. & Guo, G.-C. Computational evidence for Lewis base-promoted CO₂ hydrogenation to formic acid on gold surfaces. *ACS Catal.* **7**, 4519–4526 (2017).
47. Ren, D. et al. An unusual chemoselective hydrogenation of quinoline compounds using supported Au catalysts. *J. Am. Chem. Soc.* **134**, 17592–17598 (2012).
48. Cano, I., Chapman, A. M., Urakawa, A. & van Leeuwen, P. W. N. M. Air-stable gold nanoparticles ligated by secondary phosphine oxides for the chemoselective hydrogenation of aldehydes: crucial role of the ligand. *J. Am. Chem. Soc.* **136**, 2520–2528 (2014).
49. Cano, I. et al. Air-stable gold nanoparticles ligated by secondary phosphine oxides as catalyst for the chemoselective hydrogenation of substituted aldehydes: a remarkable ligand effect. *J. Am. Chem. Soc.* **137**, 7718–7727 (2015).
50. Garcia-Melchor, M. & Lopez, N. Homolytic products from heterolytic paths in H₂ dissociation on metal oxides: the example of CeO₂. *J. Phys. Chem. C* **118**, 10921–10926 (2014).
51. Airedy, D. & Ding, K. Heterolytic dissociation of H₂ in heterogeneous catalysis. *ACS Catal.* **12**, 4707–4723 (2022).
52. Lyalin, A. & Taketsugu, T. A computational investigation of H₂ adsorption and dissociation on Au nanoparticles supported on TiO₂ surface. *Faraday Discuss.* **152**, 185–201 (2011).
53. Du, X. et al. Size-dependent strong metal-support interaction in TiO₂ supported Au nanocatalysts. *Nat. Commun.* **11**, 5811 (2020).
54. Fu, Q., Wagner, T., Olliges, S. & Carstnanjen, H.-D. Metal–oxide interfacial reactions: encapsulation of Pd on TiO₂ (110). *J. Phys. Chem. B* **109**, 944–951 (2005).
55. Sun, Y. et al. Gold catalysts containing interstitial carbon atoms boost hydrogenation activity. *Nat. Commun.* **11**, 4600 (2020).
56. Mukherjee, S. et al. Hot-electron-induced dissociation of H₂ on gold nanoparticles supported on SiO₂. *J. Am. Chem. Soc.* **136**, 64–67 (2014).
57. Christopher, P., Xin, H., Marimuthu, A. & Linic, S. Singular characteristics and unique chemical bond activation mechanisms of photocatalytic reactions on plasmonic nanostructures. *Nat. Mater.* **11**, 1044–1050 (2012).
58. Linic, S., Christopher, P., Xin, H. & Marimuthu, A. Catalytic and photocatalytic transformations on metal nanoparticles with targeted geometric and plasmonic properties. *Acc. Chem. Res.* **46**, 1890–1899 (2013).
59. Brus, L. Noble metal nanocrystals: plasmon electron transfer photochemistry and single-molecule raman spectroscopy. *Acc. Chem. Res.* **41**, 1742–1749 (2008).
60. Quiroz, J. et al. Controlling reaction selectivity over hybrid plasmonic nanocatalysts. *Nano Lett.* **18**, 7289–7297 (2018).
61. Barbosa, E. C. M. et al. Reaction pathway dependence in plasmonic catalysis: hydrogenation as a model molecular transformation. *Chem. Eur. J.* **24**, 12330–12339 (2018).
62. Pyykkö, P. Theoretical chemistry of gold. *Angew. Chem. Int. Ed.* **43**, 4412–4456 (2004).
63. Pyykkö, P. Relativity, gold, closed-shell interactions, and CsAu–NH₃. *Angew. Chem. Int. Ed.* **41**, 3573–3578 (2002).
64. De Vos, D. & Sels, B. Gold redox catalysis for selective oxidation of methane to methanol. *Angew. Chem. Int. Ed.* **117**, 30–32 (2005).
65. Guzman, J. et al. CO oxidation catalyzed by supported Au: cooperation between gold and nanocrystalline rare-earth supports forms reactive surface superoxide and peroxide species. *Angew. Chem. Int. Ed.* **44**, 4778–4781 (2005).
66. Jones, C. et al. Selective oxidation of methane to methanol catalyzed, with C-H activation, by homogeneous, cationic gold. *Angew. Chem. Int. Ed.* **116**, 4726–4729 (2004).
67. Corma, A., Gonzalez-Arellano, C., Iglesias, M. & Sanchez, F. Gold nanoparticles and gold(III) complexes as general and selective hydrosilylation catalysts. *Angew. Chem. Int. Ed.* **19**, 7966–7968 (2007).
68. Wang, L. et al. Single-site catalyst promoters accelerate metal-catalyzed nitroarene hydrogenation. *Nat. Commun.* **9**, 1362 (2018).
69. Zhang, L., Ren, Y., Liu, W., Wang, A. & Zhang, T. Single-atom catalyst: a rising star for green synthesis of fine chemicals. *Natl. Sci. Rev.* **5**, 653–672 (2018).
70. Hannagan, R. T., Giannakakis, G., Flytzani-Stephanopoulos, M. & Sykes, E. C. Single-atom alloy catalysis. *Chem. Rev.* **120**, 12044–12088 (2020).
71. Cui, X., Li, W., Ryabchuk, P., Junge, K. & Beller, M. Bridging homogeneous and heterogeneous catalysis by heterogeneous single-metal-site catalysts. *Nat. Catal.* **1**, 385–397 (2018).
72. Cao, S. et al. Single-atom gold oxo-clusters prepared in alkaline solutions catalyze the heterogeneous methanol self-coupling reactions. *Nat. Chem.* **11**, 1098–1105 (2019).
73. Corma, A., Salnikow, O. G., Barskiy, D. A., Kovtunov, K. V. & Koptuyg, I. V. Single-atom Au catalysis in the context of developments in parahydrogen-induced polarization. *Chem. Eur. J.* **21**, 7012–7015 (2015).
74. Qiao, B. et al. Ultrastable single-atom gold catalysts with strong covalent metal-support interaction (CMSI). *Nano Res.* **8**, 2913–2924 (2015).
75. Guzman, J. & Gates, B. C. Structure and reactivity of a mononuclear gold-complex catalyst supported on magnesium oxide. *Angew. Chem. Int. Ed.* **115**, 115–114 (2003).
76. Comas-Vives, A. et al. Single-site homogeneous and heterogenized gold(III) hydrogenation catalysts: mechanistic implications. *J. Am. Chem. Soc.* **128**, 4756–4765 (2006).
77. Sárkány, A., Schay, Z., Frey, K., Széles, É. & Sajó, I. Some features of acetylene hydrogenation on Au-iron oxide catalyst. *Appl. Catal. A Gen.* **380**, 133–141 (2010).
78. Zhang, X., Shi, H. & Xu, B. Catalysis by gold: isolated surface Au³⁺ ions are active sites for selective hydrogenation of 1,3-butadiene over Au/ZrO₂ Catalysts. *Angew. Chem. Int. Ed.* **44**, 7132–7135 (2005).
79. He, X. et al. A versatile route to fabricate single atom catalysts with high chemoselectivity and regioselectivity in hydrogenation. *Nat. Commun.* **10**, 3663 (2019).
80. Single atom catalysts push the boundaries of heterogeneous catalysis. *Nat. Commun.* **12**, 5884 (2021).
81. Wang, Z., Gu, L., Song, L., Wang, H. & Yu, R. Facile one-pot synthesis of MOF supported gold pseudo-single-atom catalysts for hydrogenation reactions. *Mater. Chem. Front.* **2**, 1024–1030 (2018).
82. Liu, J. et al. Ligand–metal charge transfer induced *via* adjustment of textural properties controls the performance of single-atom catalysts during photocatalytic degradation. *ACS Appl. Mater. Interfaces* **13**, 25858–25867 (2021).
83. Vilé, G. et al. Azide-alkyne click chemistry over a heterogeneous copper-based single-atom catalyst. *ACS Catal.* **12**, 2947–2958 (2022).
84. Gan, T. et al. Unveiling the kilogram-scale gold single-atom catalysts via ball milling for preferential oxidation of CO in excess hydrogen. *Chem. Eng. J.* **389**, 124490 (2020).
85. Greeley, J. & Mavrikakis, M. Alloy catalysts designed from first principles. *Nat. Mater.* **3**, 810–815 (2004).
86. Fu, Q. & Luo, Y. Catalytic activity of single transition-metal atom doped in Cu(111) surface for heterogeneous hydrogenation. *J. Phys. Chem. C* **117**, 14618–14624 (2013).

87. Alayoglu, S., Nilekar, A. U., Mavrikakis, M. & Eichhorn, B. Ru–Pt core–shell nanoparticles for preferential oxidation of carbon monoxide in hydrogen. *Nat. Mater.* **7**, 333–338 (2008).
88. Kyriakou, G. et al. Isolated metal atom geometries as a strategy for selective heterogeneous hydrogenations. *Science* **335**, 1209–1212 (2012).
89. Boucher, M. B. et al. Single atom alloy surface analogs in Pd_{0.18}Cu_{0.15} nanoparticles for selective hydrogenation reactions. *Phys. Chem. Chem. Phys.* **15**, 12187–12196 (2013).
90. Sankar, M. et al. Designing bimetallic catalysts for a green and sustainable future. *Chem. Soc. Rev.* **41**, 8099–8139 (2012).
91. Maroun, F., Ozanam, F., Magnussen, O. M. & Behm, R. J. The role of atomic ensembles in the reactivity of bimetallic electrocatalysts. *Science* **293**, 1811–1814 (2001).
92. Venkatachalam, S. & Jacob, T. Hydrogen adsorption on Pd-containing Au(111) bimetallic surfaces. *Phys. Chem. Chem. Phys.* **11**, 3263–3270 (2009).
93. van der Hoeven, J. E. S. et al. Entropic control of H–D exchange rates over dilute Pd-in-Au alloy nanoparticle catalysts. *ACS Catal.* **11**, 6971–6981 (2021).
94. Buurmans, I. & Weckhuysen, B. Heterogeneities of individual catalyst particles in space and time as monitored by spectroscopy. *Nat. Chem.* **4**, 873–886 (2012).
95. Sambur, J. et al. Sub-particle reaction and photocurrent mapping to optimize catalyst-modified photoanodes. *Nature* **530**, 77–80 (2016).
96. Yin, H. et al. Nanometre-scale spectroscopic visualization of catalytic sites during a hydrogenation reaction on a Pd/Au bimetallic catalyst. *Nat. Catal.* **3**, 834–842 (2020).
97. Lucci, F. R. et al. Controlling hydrogen activation, spillover, and desorption with Pd–Au single-atom alloys. *J. Phys. Chem. Lett.* **7**, 480–485 (2016).
98. Liu, J. et al. Integrated catalysis-surface science-theory approach to understand selectivity in the hydrogenation of 1-hexyne to 1-hexene on PdAu single-atom alloy catalysts. *ACS Catal.* **9**, 8757–8765 (2019).
99. Shi, D. et al. Probing the core and surface composition of nanoalloy to rationalize its selectivity: study of Ni-Fe/SiO₂ catalysts for liquid-phase hydrogenation. *Chem Catal.* **2**, 1686–1708 (2022).
100. Zhang, X. et al. Reversible loss of core–shell structure for Ni–Au bimetallic nanoparticles during CO₂ hydrogenation. *Nat. Catal.* **3**, 411–417 (2020).
101. van der Hoeven, J. E. S. et al. Unlocking synergy in bimetallic catalysts by core–shell design. *Nat. Mater.* **20**, 1216–1220 (2021).
102. Luneau, M. et al. Enhancing catalytic performance of dilute metal alloy nanomaterials. *Commun. Chem.* **3**, 46 (2020).
103. Datye, A. K. & Guo, H. Single atom catalysis poised to transition from an academic curiosity to an industrially relevant technology. *Nat. Commun.* **12**, 895 (2021).
104. Zhao, X., Fang, R., Kong, X. & Li, Y. Atomic design of dual-metal hetero-single-atoms for high-efficiency synthesis of natural flavones. *Nat. Commun.* **13**, 7873 (2022).
105. Tian, S. et al. Dual-atom Pt heterogeneous catalyst with excellent catalytic performances for the selective hydrogenation and epoxidation. *Nat. Commun.* **12**, 3181 (2021).
106. Zhang, T. et al. The dual-active-site tandem catalyst containing Ru single atoms and Ni nanoparticles boosts CO₂ methanation. *Appl. Catal. B* **323**, 122190 (2023).
107. Paul Sabatier Nobel Lecture. *NobelPrize.org* <https://www.nobelprize.org/prizes/chemistry/1912/sabatier/lecture/> (2024).
108. Hastert, R. C. Hydrogenation of fatty acids. *J. Am. Oil Chem. Soc.* **56**, 732A–739A (1979).
109. Luza, L. et al. Revealing hydrogenation reaction pathways on naked gold nanoparticles. *ACS Catal.* **7**, 2791–2799 (2017).
110. Luza, L. et al. Tunneling effects in confined gold nanoparticle hydrogenation catalysts. *Phys. Chem. Chem. Phys.* **21**, 16615–16622 (2019).
111. Eom, N., Messing, M., Johansson, J. & Deppert, K. General trends in core–shell preferences for bimetallic nanoparticles. *ACS Nano* **15**, 8883–8895 (2021).
112. Ledendecker, M. et al. Engineering gold-platinum core-shell nanoparticles by self-limitation in solution. *Commun. Chem.* **5**, 71 (2022).
113. Bruno, L., Scuderi, M., Priolo, F., Falciola, L. & Mirabella, S. Enlightening the bimetallic effect of Au@Pd nanoparticles on Ni oxide nanostructures with enhanced catalytic activity. *Sci. Rep.* **13**, 3203 (2023).
114. Zhao, J. et al. Ir promotion of TiO₂ supported Au catalysts for selective hydrogenation of cinnamaldehyde. *Catal. Commun.* **54**, 72–76 (2014).
115. Li, H. et al. Improved chemoselective hydrogenation of crotonaldehyde over bimetallic AuAg/SBA-15 catalyst. *J. Catal.* **330**, 135–144 (2015).
116. Chen, J., Sun, W., Wang, Y. & Fang, W. Performant Au hydrogenation catalyst cooperated with Cu-doped Al₂O₃ for selective conversion of furfural to furfuryl alcohol at ambient pressure. *Green. Energy Environ.* **6**, 546–556 (2021).
117. Tkachenko, G., Truong, V. G., Esporas, C. L., Sanskriti, I. & Nic Chormaic, S. Evanescent field trapping and propulsion of Janus particles along optical nanofibers. *Nat. Commun.* **14**, 1691 (2023).

Acknowledgements

R.W. discloses support for publication of this work from Programme Investissement d'Avenir (I-SITE ULNE / ANR-16-IDEX-0004 ULNE), Métropole Européenne de Lille (MEL) and Region Hauts-de-France for the (CatBioInnov project).

Author contributions

The authors contributed equally to all aspects of the article.

Competing interests

The authors declare no competing interests.

Additional information

Peer review information *Nature Reviews Chemistry* thanks Mathilde Luneau, Hio Tong Ngan, Philippe Sautet and the anonymous reviewers for their contribution to the peer review of this work.

Publisher's note Springer Nature remains neutral with regard to jurisdictional claims in published maps and institutional affiliations.

Springer Nature or its licensor (e.g. a society or other partner) holds exclusive rights to this article under a publishing agreement with the author(s) or other rightsholder(s); author self-archiving of the accepted manuscript version of this article is solely governed by the terms of such publishing agreement and applicable law.

© Springer Nature Limited 2024